

Effects of New Heavy Fermions on Complex Scalar Dark Matter Phenomenology in Gauged Two Higgs Doublet Model

Bayu Dirgantara^{1,*} and Chrisna Setyo Nugroho^{2,†}

¹*School of Physics and Center of Excellence in High Energy Physics & Astrophysics,
Suranaree University of Technology,
Nakhon Ratchasima, 30000, Thailand*

²*Physics Division, National Center for Theoretical Sciences,
National Tsing-Hua University, Hsinchu, 30013, Taiwan*

Abstract

We study the inclusion of new heavy fermions on complex scalar dark matter (DM) phenomenology within gauged two Higgs doublet model (G2HDM). We find that for DM mass above 1 TeV, heavy quarks coannihilations into the Standard Model (SM) quarks and gluons dominate the thermally-averaged cross section relevant for the relic abundance of complex scalar DM. We demonstrate that the effects of QCD Sommerfeld correction as well as QCD bound state formation in determining the DM relic density are negligible. We show that the allowed parameter space is significantly constrained by the current PLANCK relic density data as well as XENON1T limit appropriate for DM direct search.

* bayuquarkquantum@yahoo.com

† csnugroho@cts.nthu.edu.tw

I. INTRODUCTION

The nature of dark matter (DM) is one of the open problems in cosmology, astrophysics and particle physics. Apart from its gravitational interaction, there is no evidence that it interacts with ordinary matter via the other existing forces in nature. Furthermore, the current understanding of our universe can be explained very well if one includes the existence of the cold DM in addition to the ordinary matter and dark energy. It has been assumed that the DM was in thermal equilibrium with the Standard Model (SM) particles in the early universe. As the reaction rate that keeps the DM in thermal equilibrium with other SM particles drops out and becomes comparable with the expansion rate of the universe, it froze-out. As a result, it remains with us today. One of the most popular and well studied DM candidates so far is the weakly interacting massive particle (WIMP). This candidate fits the observed DM abundance with the typical electroweak scale annihilation cross section.

The need to extend the SM particle contents is necessary since it does not provide any suitable DM candidate. One of the most studied examples of the SM extension is the general two Higgs doublet model (2HDM). This model comes with many variations and each of them offers different phenomenological features, see for example [1, 2] for a review. As one of the 2HDM variants, the inert Higgs doublet model (IHDM) [3] provides a suitable DM candidate. This is done by imposing the discrete \mathcal{Z}_2 symmetry in which the second Higgs doublet belongs to the \mathcal{Z}_2 -odd particle. This model has been studied in detail over the years [4–27]. Recently, this \mathcal{Z}_2 symmetry appears as an accidental symmetry in a renormalizable gauged two Higgs doublet model (G2HDM) and it has been studied in detail in [28, 29]. In this model, the two Higgs doublets are put together in a doublet representation of an additional $SU(2)_H$ gauge group. In addition to this, there is also a new $U(1)_X$ symmetry. As for the scalar sector, it is expanded by including a new $SU(2)_H$ triplet and doublet. These

new scalars transform trivially under the SM gauge group.

As in IHDM, there is a suitable scalar DM candidate in G2HDM. In this case, the stability of the DM is protected by the accidental \mathcal{Z}_2 symmetry. The phenomenological study of this DM has been done in [29]. This study has taken the previous results of the G2HDM studies [32–36] into account, especially the results from [35, 36]. These two studies put the constraints in the scalar sector and gauge sector of the G2HDM. These include vacuum stability of the scalar potential, perturbative unitarity, Higgs physics, Drell-Yan process, the Z' search, as well as electroweak precision test (EWPT). We dubbed these results as the scalar and gauge sector constraints (**SGSC**). However, the previous DM study in [29] neglects the heavy \mathcal{Z}_2 -odd fermions in their calculation. In this paper, we focus on the effects of these new heavy fermions on complex scalar DM phenomenology. For consistency with the previous DM study, we take **SGSC** constraints as our starting points.

This paper is organized as follows. In Sec. II we briefly mention the important aspects of the G2HDM model, especially the scalar potential, mass spectra, and suitable dark matter candidates. To compare our DM study against the existing experimental data, we discuss how relic density (**RD**) and direct detection (**DD**) constraint our complex scalar DM. This is discussed in Sec. III. In Sec. IV, we briefly explain the methodology employed in our numerical computation. We further discuss in detail the results obtained in our analysis. In Sec. V, we discuss QCD Sommerfeld correction and QCD bound state effect relevant for the relic density calculation. The allowed parameter space after imposing DM physics constraints is discussed in Sec. VI. Finally, we summarize and conclude our study in Sec. VII. We list the most important Feynman rules used in the discussion of this work in Appendix A.

II. THE G2HDM MODEL

A. Matter Content

Matter Fields	$SU(3)_C \times SU(2)_L \times SU(2)_H \times U(1)_Y \times U(1)_X$
$H = (H_1, H_2)^T$	(1, 2, 2, 1/2, 1)
Δ_H	(1, 1, 3, 0, 0)
Φ_H	(1, 1, 2, 0, 1)
$Q_L = (u_L, d_L)^T$	(3, 2, 1, 1/6, 0)
$U_R = (u_R, u_R^H)^T$	(3, 1, 2, 2/3, 1)
$D_R = (d_R^H, d_R)^T$	(3, 1, 2, -1/3, -1)
$L_L = (\nu_L, e_L)^T$	(1, 2, 1, -1/2, 0)
$N_R = (\nu_R, \nu_R^H)^T$	(1, 1, 2, 0, 1)
$E_R = (e_R^H, e_R)^T$	(1, 1, 2, -1, -1)
ν_L^H	(1, 1, 1, 0, 0)
e_L^H	(1, 1, 1, -1, 0)
u_L^H	(3, 1, 1, 2/3, 0)
d_L^H	(3, 1, 1, -1/3, 0)

TABLE I. Matter contents and their corresponding quantum numbers in G2HDM. New heavy fermions are denoted by the superscript H .

The gauge group of G2HDM is realized by expanding the SM gauge symmetry with additional $SU(2)_H \times U(1)_X$ dubbed as hidden gauge sector. The SM scalar sector H_1 is extended by adding one Higgs doublet H_2 in such a way that both of them transform under the fundamental representation of $SU(2)_L$ and $SU(2)_H$ gauge group. Furthermore, Δ_H and Φ_H , which transform under the triplet and doublet

representations of $SU(2)_H$, are present. Both of them are SM singlets.

New right-handed heavy fermions are put together with the SM right-handed fermions into $SU(2)_H$ doublets while maintaining the trivial representation of $SU(2)_L$. Furthermore, anomaly cancellation dictates us to further include two pairs of left-handed heavy quarks and two pairs of left-handed heavy leptons for each generation, which are singlets under $SU(2)$ and $U(1)_X$. As a remark, one notes that the $SU(2)_H$ considered here is different from the $SU(2)_R$ in left-right symmetric models [38, 39]. The $W'^{(p,m)}$ in G2HDM is electrically neutral, while the W'^{\pm} in left-right symmetric carry non-zero electric charges. This is the rationale behind the superscripts p and m in labelling W' . As another comparison, we also observe that non-sterile right-handed neutrinos ν_{lRS} , incorporated in the mirror fermion models of electroweak scale right-handed neutrinos [40–45], are different from our setup. In the mirror fermion models, ν_{lRS} are paired together with mirror charged leptons l_R^M s to form $SU(2)_L$ doublets. In contrast, they are grouped with new heavy right-handed neutrinos ν_{lR}^H to form $SU(2)_H$ doublets in G2HDM. There are several models that impose additional gauge symmetry on 2HDM to solve flavor problem, dark matter and neutrino masses, see for instance [46–51]. In table I, we list the matter contents of the G2HDM model and their associated quantum numbers.

B. Scalar Potential and Mass Spectra

Scalar Potential

The most general renormalizable scalar potential that satisfies the G2HDM symmetries comprises 4 distinct terms [35]

$$V_T = V(H) + V(\Phi_H) + V(\Delta_H) + V_{\text{mix}}(H, \Delta_H, \Phi_H) . \quad (1)$$

The first term $V(H)$ in Eq. (1) contains self-interaction of $SU(2)_L$ and $SU(2)_H$ scalar doublet H reads as

$$\begin{aligned}
V(H) &= \mu_H^2 (H^{\alpha i} H_{\alpha i}) + \lambda_H (H^{\alpha i} H_{\alpha i})^2 + \frac{1}{2} \lambda'_H \epsilon_{\alpha\beta} \epsilon^{\gamma\delta} (H^{\alpha i} H_{\gamma i}) (H^{\beta j} H_{\delta j}) \\
&= \mu_H^2 (H_1^\dagger H_1 + H_2^\dagger H_2) + \lambda_H (H_1^\dagger H_1 + H_2^\dagger H_2)^2 \\
&\quad + \lambda'_H (-H_1^\dagger H_1 H_2^\dagger H_2 + H_1^\dagger H_2 H_2^\dagger H_1) , \quad (2)
\end{aligned}$$

where Greek and Latin letters indicate $SU(2)_H$ and $SU(2)_L$ indices respectively, both of which run from 1 to 2, and the upper and lower indices are related by complex conjugation, i.e., $H^{\alpha i} = H_{\alpha i}^*$. A close inspection shows that the second line of Eq. (2) exhibits the discrete \mathcal{Z}_2 symmetry of $H_1 \rightarrow H_1$ and $H_2 \rightarrow -H_2$. The appearance of this discrete symmetry in G2HDM model is more natural unlike the discrete symmetry in general 2HDM model. In the latter case, one needs to put this symmetry by hand to forbid FCNC at tree level in the Yukawa sectors. The second term $V(\Phi_H)$ is the self interaction of Φ_H

$$\begin{aligned}
V(\Phi_H) &= \mu_\Phi^2 \Phi_H^\dagger \Phi_H + \lambda_\Phi (\Phi_H^\dagger \Phi_H)^2 \\
&= \mu_\Phi^2 (\Phi_1^* \Phi_1 + \Phi_2^* \Phi_2) + \lambda_\Phi (\Phi_1^* \Phi_1 + \Phi_2^* \Phi_2)^2 , \quad (3)
\end{aligned}$$

where $\Phi_H = (\Phi_1, \Phi_2)^T$ belongs to the $SU(2)_H$ doublet. The self interaction of the $SU(2)_H$ scalar triplet Δ_H reads

$$\begin{aligned}
V(\Delta_H) &= -\mu_\Delta^2 \text{Tr} (\Delta_H^2) + \lambda_\Delta (\text{Tr} (\Delta_H^2))^2 \\
&= -\mu_\Delta^2 \left(\frac{1}{2} \Delta_3^2 + \Delta_p \Delta_m \right) + \lambda_\Delta \left(\frac{1}{2} \Delta_3^2 + \Delta_p \Delta_m \right)^2 , \quad (4)
\end{aligned}$$

where the triplet field is expressed as

$$\Delta_H = \begin{pmatrix} \Delta_3/2 & \Delta_p/\sqrt{2} \\ \Delta_m/\sqrt{2} & -\Delta_3/2 \end{pmatrix} = \Delta_H^\dagger \text{ with } \Delta_m = (\Delta_p)^* \text{ and } (\Delta_3)^* = \Delta_3 . \quad (5)$$

Here, the off-diagonal components of the $SU(2)_H$ triplet, Δ_H , are electrically neutral. Following the same labelling as in $W^{(p,m)}$, we put the subscripts p and m on them. Finally, the last term V_{mix} takes all possible mixing between H , Φ_H as well as Δ_H into account, and it is given by

$$\begin{aligned}
V_{\text{mix}}(H, \Delta_H, \Phi_H) = & + M_{H\Delta} (H^\dagger \Delta_H H) - M_{\Phi\Delta} (\Phi_H^\dagger \Delta_H \Phi_H) \\
& + \lambda_{H\Phi} (H^\dagger H) (\Phi_H^\dagger \Phi_H) + \lambda'_{H\Phi} (H^\dagger \Phi_H) (\Phi_H^\dagger H) \\
& + \lambda_{H\Delta} (H^\dagger H) \text{Tr}(\Delta_H^2) + \lambda_{\Phi\Delta} (\Phi_H^\dagger \Phi_H) \text{Tr}(\Delta_H^2) . \quad (6)
\end{aligned}$$

The explicit expression of Eq. (6) in terms of its components is

$$\begin{aligned}
V_{\text{mix}}(H, \Delta_H, \Phi_H) = & + M_{H\Delta} \left(\frac{1}{\sqrt{2}} H_1^\dagger H_2 \Delta_p + \frac{1}{2} H_1^\dagger H_1 \Delta_3 + \frac{1}{\sqrt{2}} H_2^\dagger H_1 \Delta_m - \frac{1}{2} H_2^\dagger H_2 \Delta_3 \right) \\
& - M_{\Phi\Delta} \left(\frac{1}{\sqrt{2}} \Phi_1^* \Phi_2 \Delta_p + \frac{1}{2} \Phi_1^* \Phi_1 \Delta_3 + \frac{1}{\sqrt{2}} \Phi_2^* \Phi_1 \Delta_m - \frac{1}{2} \Phi_2^* \Phi_2 \Delta_3 \right) \\
& + \lambda_{H\Phi} (H_1^\dagger H_1 + H_2^\dagger H_2) (\Phi_1^* \Phi_1 + \Phi_2^* \Phi_2) \\
& + \lambda'_{H\Phi} (H_1^\dagger H_1 \Phi_1^* \Phi_1 + H_2^\dagger H_2 \Phi_2^* \Phi_2 + H_1^\dagger H_2 \Phi_2^* \Phi_1 + H_2^\dagger H_1 \Phi_1^* \Phi_2) \\
& + \lambda_{H\Delta} (H_1^\dagger H_1 + H_2^\dagger H_2) \left(\frac{1}{2} \Delta_3^2 + \Delta_p \Delta_m \right) \\
& + \lambda_{\Phi\Delta} (\Phi_1^* \Phi_1 + \Phi_2^* \Phi_2) \left(\frac{1}{2} \Delta_3^2 + \Delta_p \Delta_m \right) . \quad (7)
\end{aligned}$$

As before, $V_{\text{mix}}(H, \Delta_H, \Phi_H)$ is also invariant under $H_1 \rightarrow H_1$, $H_2 \rightarrow -H_2$, $\Phi_1 \rightarrow -\Phi_1$, $\Phi_2 \rightarrow \Phi_2$, $\Delta_3 \rightarrow \Delta_3$, and $\Delta_{p,m} \rightarrow -\Delta_{p,m}$. It has been shown in [29] that this discrete symmetry holds in all sector in G2HDM.

C. Mass Spectra

The gauge symmetry of G2HDM is broken spontaneously by the vacuum expectation values (VEVs) of $\langle H_1 \rangle = (0, v/\sqrt{2})^T$, $\langle \Phi_2 \rangle = v_\Phi/\sqrt{2}$, and $\langle \Delta_3 \rangle = -v_\Delta$ [28, 35].

As a result of this spontaneous symmetry breaking (SSB), all fields in G2HDM acquire their mass from these VEVs. In this subsection, we discuss the mass spectra of G2HDM, focusing mainly on the scalar and gauge sector.

Higgs-like (\mathcal{Z}_2 -even) Scalars

The mass terms as well as the mixing terms of the scalar fields can be extracted by writing the scalar potential in terms of the existing VEVs and further taking the second derivatives with respect to the corresponding scalar fields. The SM Higgs can be obtained from the mixing of three real scalars h , ϕ_2 and δ_3 ¹. In the basis of $\mathcal{S} = \{h, \phi_2, \delta_3\}^T$, the corresponding mixing matrix of these \mathcal{Z}_2 -even neutral real scalars is

$$\mathcal{M}_0^2 = \begin{pmatrix} 2\lambda_H v^2 & \lambda_{H\Phi} v v_\Phi & \frac{v}{2} (M_{H\Delta} - 2\lambda_{H\Delta} v_\Delta) \\ \lambda_{H\Phi} v v_\Phi & 2\lambda_\Phi v_\Phi^2 & \frac{v_\Phi}{2} (M_{\Phi\Delta} - 2\lambda_{\Phi\Delta} v_\Delta) \\ \frac{v}{2} (M_{H\Delta} - 2\lambda_{H\Delta} v_\Delta) & \frac{v_\Phi}{2} (M_{\Phi\Delta} - 2\lambda_{\Phi\Delta} v_\Delta) & \frac{1}{4v_\Delta} (8\lambda_\Delta v_\Delta^3 + M_{H\Delta} v^2 + M_{\Phi\Delta} v_\Phi^2) \end{pmatrix}. \quad (8)$$

This matrix is diagonalized by using an orthogonal matrix \mathcal{O} to obtain the masses of the physical fields as

$$\mathcal{O}^T \cdot \mathcal{M}_0^2 \cdot \mathcal{O} = \text{Diag}(m_{h_1}^2, m_{h_2}^2, m_{h_3}^2), \quad (9)$$

where the masses of the fields are ordered as $m_{h_1} \leq m_{h_2} \leq m_{h_3}$. The interaction basis \mathcal{S} and the mass eigenfields are linked to each other via \mathcal{O} as $\mathcal{S} = \mathcal{O} \cdot \{h_1, h_2, h_3\}^T$. The 125 GeV SM Higgs is chosen to be the lightest mass eigenstate h_1 .

¹ We parameterize the scalar fields as the notations of [28]: $H_1 = \begin{pmatrix} G^+ \\ \frac{v+h}{\sqrt{2}} + iG^0 \end{pmatrix}$, $H_2 = \begin{pmatrix} H^+ \\ H_2^0 \end{pmatrix}$,

$$\Phi_H = \begin{pmatrix} G_H^p \\ \frac{v_\Phi + \phi_2}{\sqrt{2}} + iG_H^0 \end{pmatrix}, \text{ and } \Delta_H = \begin{pmatrix} \frac{-v_\Delta + \delta_3}{2} & \frac{\Delta_p}{\sqrt{2}} \\ \frac{\Delta_m}{\sqrt{2}} & \frac{v_\Delta - \delta_3}{2} \end{pmatrix}.$$

The remaining \mathcal{Z}_2 -even scalars $G^{\pm,0}$ and G_H^0 do not mix with the existing scalar fields. These would be Goldstone bosons will be absorbed by the gauge bosons.

Dark (\mathcal{Z}_2 -odd) Scalars

The mass of the charged Higgs can be read directly from the scalar potential since it does not mix with other scalars in G2HDM. Since it interacts with H_1 , Φ_H as well as Δ_H , the charged Higgs receives its mass from the VEVs of these fields as

$$m_{H^\pm}^2 = M_{H\Delta}v_\Delta - \frac{1}{2}\lambda'_H v^2 + \frac{1}{2}\lambda'_{H\Phi}v_\Phi^2. \quad (10)$$

On the other hand, the three neutral complex fields $G_H^{p,m}$, $H_2^{0(*)}$ and $\Delta_{p,m}$ ² mix with each other as

$$\mathcal{M}_0^2 = \begin{pmatrix} M_{\Phi\Delta}v_\Delta + \frac{1}{2}\lambda'_{H\Phi}v^2 & \frac{1}{2}\lambda'_{H\Phi}vv_\Phi & -\frac{1}{2}M_{\Phi\Delta}v_\Phi \\ \frac{1}{2}\lambda'_{H\Phi}vv_\Phi & M_{H\Delta}v_\Delta + \frac{1}{2}\lambda'_{H\Phi}v_\Phi^2 & \frac{1}{2}M_{H\Delta}v \\ -\frac{1}{2}M_{\Phi\Delta}v_\Phi & \frac{1}{2}M_{H\Delta}v & \frac{1}{4v_\Delta}(M_{H\Delta}v^2 + M_{\Phi\Delta}v_\Phi^2) \end{pmatrix}, \quad (11)$$

where this matrix is written in the basis of $\mathcal{G} = \{G_H^p, H_2^{0*}, \Delta_p\}^T$. As one can easily check from its determinant, this mass matrix has at least one zero eigenvalue. Upon diagonalization, the interaction basis and mass basis are related via orthogonal matrix \mathcal{O}^D as $\mathcal{G} = \mathcal{O}^D \cdot \{\tilde{G}^p, D, \tilde{\Delta}\}^T$ such that the orthogonal matrix \mathcal{O}^D brings the mixing matrix into the diagonal form

$$(\mathcal{O}^D)^T \cdot \mathcal{M}_0^2 \cdot \mathcal{O}^D = \text{Diag}(0, m_D^2, m_{\tilde{\Delta}}^2). \quad (12)$$

The complex gauge bosons $SU(2)_H$, $W^{(p,m)}$, become massive by absorbing the first zero eigenvalue in Eq. (12), i.e., $\tilde{G}^{p,m}$, into their longitudinal component. Here, the hierarchy $m_D^2 < m_{\tilde{\Delta}}^2$ has been assumed. In order to facilitate the analysis in the

² See the previous footnote for the definitions of these complex scalars.

case when D is the dark matter candidate, we have excluded $m_D = m_{\tilde{\Delta}}$ case. This degenerate in masses happens actually under the very special condition as can be inferred from the mass formula of the two physical states given below

$$M_{D,\tilde{\Delta}}^2 = \frac{-B \mp \sqrt{B^2 - 4AC}}{2A}, \quad (13)$$

where

$$\begin{aligned} A &= 8v_{\Delta}, \\ B &= -2 [M_{H\Delta} (v^2 + 4v_{\Delta}^2) + M_{\Phi\Delta} (4v_{\Delta}^2 + v_{\Phi}^2) + 2\lambda'_{H\Phi} v_{\Delta} (v^2 + v_{\Phi}^2)] , \\ C &= (v^2 + v_{\Phi}^2 + 4v_{\Delta}^2) [M_{H\Delta} (\lambda'_{H\Phi} v^2 + 2M_{\Phi\Delta} v_{\Delta}) + \lambda'_{H\Phi} M_{\Phi\Delta} v_{\Phi}^2] . \end{aligned} \quad (14)$$

As can be seen from this formula, the degeneracy between D and $\tilde{\Delta}$ occurs when the argument under the square root vanishes. Furthermore, we require $m_{H^{\pm}} > m_D$ to make D a suitable DM candidate.

Gauge Bosons

Once the SSB takes place, all the gauge fields W , W' , B , and X become massive. The charged SM gauge boson, W^{\pm} , doesn't mix with other gauge bosons. Its mass is completely determined by the VEV of H_1 as $m_{W^{\pm}} = gv/2$. On the other hand, the neutral gauge boson coming from the off-diagonal component of $SU(2)_H$, $W'^{(p,m)}$, receives its mass from all existing VEVs as

$$m_{W'^{(p,m)}}^2 = \frac{1}{4} g_H^2 (v^2 + v_{\Phi}^2 + 4v_{\Delta}^2). \quad (15)$$

The neutral gauge bosons corresponding to the third generator of the $SU(2)_L$ and $SU(2)_H$, W^3 and W'^3 , mix with B as well as X . In the basis of $\mathcal{V}' =$

$\{B, W^3, W'^3, X\}^T$, their mixing matrix is given by the following 4×4 matrix

$$\mathcal{M}_1^2 = \begin{pmatrix} \frac{g'^2 v^2}{4} + M_Y^2 & -\frac{g' g v^2}{4} & \frac{g' g_H v^2}{4} & \frac{g' g_X v^2}{2} + M_X M_Y \\ -\frac{g' g v^2}{4} & \frac{g^2 v^2}{4} & -\frac{g g_H v^2}{4} & -\frac{g g_X v^2}{2} \\ \frac{g' g_H v^2}{4} & -\frac{g g_H v^2}{4} & \frac{g_H^2 (v^2 + v_\Phi^2)}{4} & \frac{g_H g_X (v^2 - v_\Phi^2)}{2} \\ \frac{g' g_X v^2}{2} + M_X M_Y & -\frac{g g_X v^2}{2} & \frac{g_H g_X (v^2 - v_\Phi^2)}{2} & g_X^2 (v^2 + v_\Phi^2) + M_X^2 \end{pmatrix}, \quad (16)$$

where M_X and M_Y stand for two Stueckelberg mass parameters [52–60] associated with $U(1)_X$ and $U(1)_Y$, respectively. The determinant of this matrix is zero. As a consequence, there is at least one massless eigenstate which can be associated with the photon. We set $M_Y = 0$ to avoid a non-zero electric charges of the neutrinos as discussed in [36]. Moreover, this particular choice allows us to bring the matrix in Eq. (16) into the following form

$$\mathcal{M}_Z^2 = \begin{pmatrix} 0 & 0 & 0 & 0 \\ 0 & M_{Z^{\text{SM}}}^2 & -\frac{g_H v}{2} M_{Z^{\text{SM}}} & -g_X v M_{Z^{\text{SM}}} \\ 0 & -\frac{g_H v}{2} M_{Z^{\text{SM}}} & \frac{g_H^2 (v^2 + v_\Phi^2)}{4} & \frac{g_X g_H (v^2 - v_\Phi^2)}{2} \\ 0 & -g_X v M_{Z^{\text{SM}}} & \frac{g_X g_H (v^2 - v_\Phi^2)}{2} & g_X^2 (v^2 + v_\Phi^2) + M_X^2 \end{pmatrix} \quad (17)$$

where $M_{Z^{\text{SM}}} = \sqrt{g^2 + g'^2} v/2$ is the SM gauge boson Z^{SM} mass. This is done by applying Weinberg rotation using the following matrix to the Eq. (16)

$$\mathcal{O}^W = \begin{pmatrix} c_W & -s_W & 0 & 0 \\ s_W & c_W & 0 & 0 \\ 0 & 0 & 1 & 0 \\ 0 & 0 & 0 & 1 \end{pmatrix}, \quad (18)$$

i.e., $(\mathcal{O}^W)^T \cdot \mathcal{M}_1^2(M_Y = 0) \cdot \mathcal{O}^W$. As a result of this rotation, we get the massless photon associated with the first component of the basis of this matrix while the second component gives us the Z^{SM} . In this case, we have the intermediate basis

$\mathcal{V}'_Z = \{A, Z^{SM}, W'^3, X\}^T$. Thus, one can express the original rotation matrix as $\mathcal{O}_{4 \times 4}^G(M_Y = 0) = \mathcal{O}^W \cdot \mathcal{O}^Z$, where the matrix \mathcal{O}^Z brings \mathcal{M}_Z^2 in Eq. (17) into a diagonal form. Consequently, the relation between the mass eigenstates and the intermediates states is given by $\mathcal{V}'_Z = \mathcal{O}^Z \cdot \{A, Z, Z', Z''\}^T$. For the rest of the paper, we assign \mathcal{O}^G to the non-diagonal 3×3 part of \mathcal{O}^Z , such that $\mathcal{O}_{j+1, k+1}^Z = \mathcal{O}_{j, k}^G$ with j and $k = 1, 2, 3$, as explicitly given in Eq. (6) of Ref. [36]. As a remark, the photon A stays the same between the intermediate states \mathcal{V}'_Z and the mass eigenstates. This implies that the only non-vanishing component in the first row and column of \mathcal{O}^Z is $\mathcal{O}_{1,1}^Z = 1$.

D. Dark Matter Candidate

As we mentioned in the preceding sections, the stability of the DM in G2HDM is protected by accidental \mathcal{Z}_2 symmetry. This symmetry, also known as the hidden parity (h -parity), is respected by all sector in G2HDM even after the SSB [28, 29]. In addition, this parity also forbids FCNC [61, 62] to occur at tree level for the SM in this model. All particles in G2HDM can be classified according to this parity as shown in Table II.

Fields	h -parity
$h, G^{\pm,0}, \phi_2, G_H^0, \delta_3, f, W_{1,2,3}^\mu, B_\mu, X^\mu, W_3^{\mu'}, G^{\mu a}$	1
$G_H^{p,m}, H_2^0, H_2^{0*}, H^\pm, \Delta_{p,m}, f^H, W_{1,2}^{\mu'}$	-1

TABLE II. Classification of all the fields in G2HDM under h -parity.

In principle, all particles with zero electric charge and have h -parity equal to -1 are suitable DM candidates. Accordingly, from Table II, the heavy neutrinos ν^H , neutral gauge boson $W'^{(p,m)}$, and the physical complex scalar D satisfy these requirements. In this work, we focus on complex scalar D as our DM candidate. The

mass mixing matrix in Eq. (11) shows that the DM candidate mass eigenstate, D , is linear combination of the interaction eigenstates G_H^p , H_2^{0*} , and Δ_p . Mathematically, this linear superposition is given by

$$D = \mathcal{O}_{12}^D G_H^p + \mathcal{O}_{22}^D H_2^{0*} + \mathcal{O}_{32}^D \Delta_p, \quad (19)$$

where \mathcal{O}_{ij}^D is the (i, j) -th component of the rotation matrix \mathcal{O}^D . The values of these components depend on the numerical values of the parameters in Eq. (11).

Following Ref [29], we classify our complex scalar DM candidate into three distinct cases: inert doublet-like DM, triplet-like DM, and Goldstone boson-like DM. This classification depends on the dominant component of the gauge eigenstate which can be characterized by the magnitude of \mathcal{O}_{ij}^D in Eq. (19). We have inert doublet-like DM if $f_{H_2} \equiv (\mathcal{O}_{22}^D)^2 > 2/3$. Triplet-like DM is achieved if $f_{\Delta_p} \equiv (\mathcal{O}_{32}^D)^2 > 2/3$. Goldstone-like DM is characterized by $f_{G^p} \equiv (\mathcal{O}_{12}^D)^2 > 2/3$. The magnitude of the \mathcal{O}_{ij}^D elements in Eq.(19) satisfy the following relation $f_{G^p} + f_{H_2} + f_{\Delta_p} = 1$.

In addition, there is another condition that holds for the Goldstone-like DM. In this case, the value of f_{G^p} must satisfy $0.67 < f_{G^p} < 0.8$ which is derived from both EWPT constraint and non-tachyonic DM mass solution as discussed in [29]. Here, we focus on triplet-like DM and Goldstone-like DM. The Inert doublet-like DM has been ruled out since it can not survive the relic density and direct detection constraints [29].

III. DARK MATTER EXPERIMENTAL CONSTRAINTS

To understand the properties of DM, we evaluate the DM-SM interactions via the existing experimental results. These include the observed DM relic abundance and the limit set by the null result coming from DM direct search. In this paper, we focus only on these two constraints as they provide the most stringent limit on the

complex scalar DM phenomenology based on the previous study in [29]. Here, we discuss the general feature of these experimental limits used in this work.

A. Relic Density

Since the interaction between DM and SM is very weak in most of the models, the observed relic abundance will be typically large. However, there exist some mechanisms other than DM self annihilations which enable us to reach the observed abundance.

First, thanks to the common \mathcal{Z}_2 -odd quantum number, DM coannihilates with other \mathcal{Z}_2 -odd particles if their mass splitting is small (typically $\lesssim 10\%$) such that their number densities do not suffer the Boltzmann suppression. In this work, coannihilations occur mainly between D and new heavy fermions f^H . This happens because of 5% mass splitting that we impose on heavy fermions. Furthermore, as we will see later, this coannihilation is dominated by heavy fermions annihilation, especially heavy quarks-anti quarks pair ($q^H \bar{q}^H$) annihilate into $q\bar{q}$ and gg . Here, $q\bar{q}$ and gg denote SM quarks and gluon, respectively.

Second, the presence of SM Higgs and heavy Higgs h_2 resonances significantly increase the thermally-averaged DM annihilation cross section. In G2HDM, this mechanism allows us to reach the correct relic abundance.

We use the most recent result provided by the PLANCK collaboration [63] for the relic density, $\Omega h^2 = 0.120 \pm 0.001$, to restrict our thermal relic calculation. Moreover, we set an additional condition on the parameter space of G2HDM to reproduce this result within 2σ significance.

B. Direct Detection

The most up to date limit for DM direct search is provided by the XENON1T collaboration [64]. The zero signal result from this experiment strongly restricts the DM nucleon cross section, in particular, in the mass regime between 10 GeV to 100 GeV. Furthermore, for DM mass around 25 GeV, they ruled out the DM-nucleon elastic cross sections which have the value larger than 10^{-46} cm².

In G2HDM, it has been shown that the interaction between DM and nucleon exhibits isospin violation (ISV) [29]. In this case, the ratio between DM-neutron to DM-proton effective coupling, f_n/f_p , is not equal to 1. This occurs due to the Z_i bosons mediated interaction. As an example, for SM Z exchange, the vectorial coupling between quark q (d or u -type) and Z is given by [29]

$$g_{\bar{q}qZ}^V = \frac{i}{2} \left[\frac{g}{c_W} (T_3 - 2Q_q s_W^2) \mathcal{O}_{11}^G + g_H T_3' \mathcal{O}_{21}^G + g_X X \mathcal{O}_{31}^G \right]. \quad (20)$$

Here, Q_q , T_3 , T_3' and X stand for the electric charge, the third generator of $SU(2)_L$, the third generator of $SU(2)_L$, and the generator of $U(1)_X$, respectively. Since the u and d quark have distinct quantum number assignments with respect to the underlying gauge group, they couple to the SM Z differently.

In order to accommodate the ISV, we need to calculate the DM-nucleus elastic scattering cross section σ_{DN}

$$\sigma_{DN} = \frac{4\mu_{\mathcal{A}}^2}{\pi} [f_p \mathcal{Z} + f_n (\mathcal{A} - \mathcal{Z})]^2, \quad (21)$$

where \mathcal{N} denotes a nucleus with mass number \mathcal{A} and proton number \mathcal{Z} and $\mu_{\mathcal{A}} = m_D m_{\mathcal{A}} / (m_D + m_{\mathcal{A}})$ is the reduced mass for DM-nucleus system. For definiteness, we neglect all the isotopes of xenon and fix \mathcal{A} and \mathcal{Z} to 131 and 54, respectively. To extract the DM-nucleon effective couplings f_n and f_p , we employ `micrOMEGAs` [65] in our computation. To compare against the limit given by XENON1T which assumes

$f_n = f_p$ in their analysis, we need to reconstruct their result at the nucleus level. In order to do so, we follow the same procedure in [29] and obtain the following expression for general value of f_n/f_p

$$\sigma_{DN}^{\text{X1T}} = \sigma_p^{\text{SI}}(\text{X1T}) \times \frac{\mu_A^2}{\mu_p^2} \times \left[\mathcal{Z} + \frac{f_n}{f_p} (\mathcal{A} - \mathcal{Z}) \right]^2, \quad (22)$$

where μ_p^2 is the DM-proton reduced mass. In this paper, we use Eq. (22) to constrain our direct detection prediction.

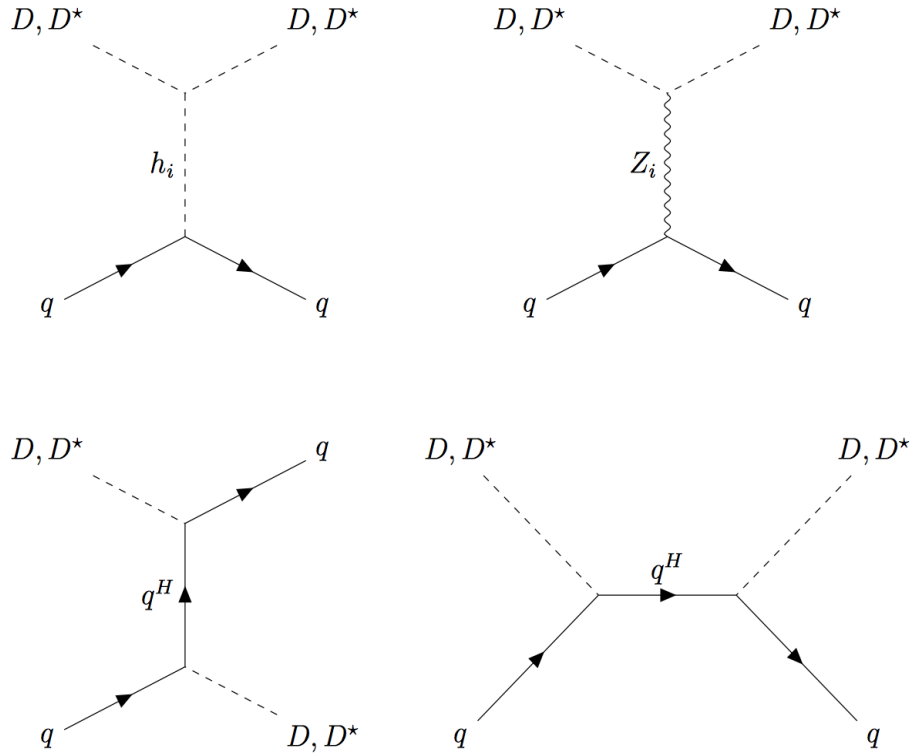


FIG. 1. The Feynman diagrams relevant for DM direct search. They consist of three t-channel diagrams with the \mathcal{Z}_2 -even Higgs bosons (top left), neutral gauge bosons (top right) and heavy quarks (bottom left) mediators. There is also s-channel heavy quarks exchange (bottom right).

In general, the DM-nucleon interaction will be different from antiDM-nucleon interaction. The spin independent interaction for complex scalar DM can be obtained by using the effective operator language as [66]

$$\mathcal{L}_D = 2\lambda_{N,e}M_D DD^* \bar{\psi}_N \psi_N + i\lambda_{N,o} \left(D^* \overleftrightarrow{\partial}_\mu D \right) \bar{\psi}_N \gamma^\mu \psi_N, \quad (23)$$

where the ψ_N , $\lambda_{N,e}$, and $\lambda_{N,o}$ stand for the nucleon field operator, the coupling of even operator, and the coupling of odd operator, respectively. In this case, the effective coupling between DM (antiDM) and the nucleon is

$$\lambda_N = \frac{\lambda_{N,e} \pm \lambda_{N,o}}{2}, \quad (24)$$

where the plus (minus) sign denotes DM-nucleon (antiDM-nucleon) interaction. Under the interchange between D and D^* , the first (second) term in the right hand side of Eq. (23) stays the same (flips sign). Because of this, the first term is called *even* operator while the second term describes *odd* operator. As a consequence, the strength of the interaction between DM-nucleon and antiDM-nucleon is different and it is given by Eq. (24). Hence, the value of σ_{D^*N} is in general not equal to σ_{DN} given by Eq. (21) because the effective couplings f_p and f_n for D are different from those for D^* . In this work, we average the contribution from both σ_{DN} and σ_{D^*N} when comparing our calculation with the XENON1T result given in Eq. (22).

The Feynman diagrams relevant for describing DM-quark interactions in G2HDM are shown in Fig. 1. For the upper part, the left panel is the t -channel interaction mediated by three Higgs bosons while the right panel is the t -channel with three neutral gauge bosons exchange. In addition, heavy quarks exchange via s and t-channel are shown in the lower part of the same figure. There is a destructive interference between heavy quarks diagrams and the Higgs mediated diagrams in triplet-like DM (Δ_p). On the other hand, the diagrams with the neutral gauge bosons and heavy quarks mediators add up constructively in Goldstone boson-like DM (G_H^p).

IV. NUMERICAL ANALYSIS AND RESULTS

A. Methodology

Taking into account the various constraints based on previous G2HDM studies, we collect a sample of points by doing random scans. These points pass the scalar sector constraints studied in [35] as we mentioned in the preceding section. In addition, we also impose the limits from the gauge sector carried out in [36]. This study includes Drell-Yan constraint which restricts the $SU(2)_H$ gauge coupling, g_H , below 0.1. To prevent the decay of DM into W' , we impose the condition $m_{W'} > m_D$ which translates into the lower bound of g_H [29]

$$g_{H\min} = \frac{2m_D}{\sqrt{v^2 + v_\Phi^2 + 4v_\Delta^2}}, \quad (25)$$

where we have used Eq. (15). The search of Z' enforces us to scan v_Φ in the mass range between 20 TeV to 100 TeV [36]. Moreover, we fix $M_X = 2$ TeV to satisfy heavy M_X scenario while maintaining the SM-like Z to 91.1876 ± 0.0021 GeV within 3σ significance [36].

In this work, we set the lower limit of heavy fermions masses to be no less than 1.0 TeV based on the signal search of the G2HDM new gauge bosons performed in [33]. In previous work [29], the lower limit is 1.5 TeV taking from the search of SUSY colored particles [37]. Also, we set the new Yukawa couplings, which are related to the new heavy fermion masses by ³ $m_{f^H} = y_{f^H} v_\Phi / \sqrt{2}$, to be small enough in order to suppress their contributions on perturbative unitarity and renormalization group running effects. In addition, the 5% mass splitting between the DM D and heavy fermions f^H is imposed here. This allows us to study their effects on DM

³ In this study, the identity matrix is used to account for the mixing between different flavors of SM and heavy fermions with the Z_2 -odd scalars in the new Yukawa sectors.

phenomenology which is the main focus of this paper. In contrast, the 20% mass splitting was imposed in [29]. To accommodate all of these requirements, we adopt the Yukawa couplings for each point in our random scan as follows

$$y_{fH} = \max \left[\frac{1.0 \text{ TeV}}{v_\Phi/\sqrt{2}}, \min \left(\frac{1.05 m_D}{v_\Phi/\sqrt{2}}, 1 \right) \right]. \quad (26)$$

From this formula, it is easy to see that the value of y_{fH} is always less than 1 for all parameters space. Based on this setup, heavy fermions are expected to give dominant contribution to the DM coannihilation.

Approximately, 3 million points are collected from our random scan. These points cover all numerical values for model parameters, gauge bosons and scalar masses, as well as all components of three mixing matrices \mathcal{O} , \mathcal{O}^D and \mathcal{O}^G . Furthermore, we input these numbers to `MicrOMEGAs` [65] to compute DM relic density and DM-nucleon cross section.

The scan range for our computation is tabulated in Table III. Note that $M_{H\Delta}$, $M_{\Phi\Delta}$, v_Δ and v_Φ have distinctive ranges for the associated DM composition. These differences are remarkable in the case of v_Δ and v_Φ in the Goldstone-like column which exhibits a fine-tuning. This happens because the Goldstone-like composition is achievable only when $0.8 \leq v_\Delta/v_\Phi < 0.9$ as discussed in [29].

B. Results

Here, we discuss the analysis of our numerical results. We evaluate the effects of heavy fermions on DM phenomenology for triplet-like DM and Goldstone-like DM separately.

Parameter	Triplet-like	Goldstone-like
λ_H	[0.12, 2.75]	[0.12, 2.75]
λ_Φ	[10^{-4} , 4.25]	[10^{-4} , 4.25]
λ_Δ	[10^{-4} , 5.2]	[10^{-4} , 5.2]
$\lambda_{H\Phi}$	[-6.2, 4.3]	[-6.2, 4.3]
$\lambda_{H\Delta}$	[-4.0, 10.5]	[-4.0, 10.5]
$\lambda_{\Phi\Delta}$	[-5.5, 15.0]	[-5.5, 15.0]
$\lambda'_{H\Phi}$	[-1.0, 18.0]	[-1.0, 18.0]
λ'_H	[$-8\sqrt{2}\pi$, $8\sqrt{2}\pi$]	[$-8\sqrt{2}\pi$, $8\sqrt{2}\pi$]
g_H	[See text, 0.1]	[See text, 0.1]
g_X	[10^{-8} , 1.0]	[10^{-8} , 1.0]
$M_{H\Delta}/\text{GeV}$	[-3000, 5000]	[0.0, 5000]
$M_{\Phi\Delta}/\text{GeV}$	[-50.0, 50.0]	[0.0, 700]
v_Δ/TeV	[0.5, 20.0]	[14.0, 20.0]
v_Φ/TeV	[20, 100]	[20, 28.0]

TABLE III. Parameter ranges used in the numerical scans that pass **SGSC** constraints. Here, M_X is fixed at 2 TeV and $M_Y = 0$.

SU(2)_H Triplet-like DM

The scatter plots for the relic density versus DM mass m_D in the triplet-like DM are presented in Fig. 2. The red line represents the observed relic density provided by the PLANCK collaboration. The right panel takes heavy fermions contributions into account while the left is adopted from [29]. Let us elaborate more by considering different DM mass regimes.

- (i) We start with the lower DM mass regime ranging from 1 GeV to 62.5 GeV. In

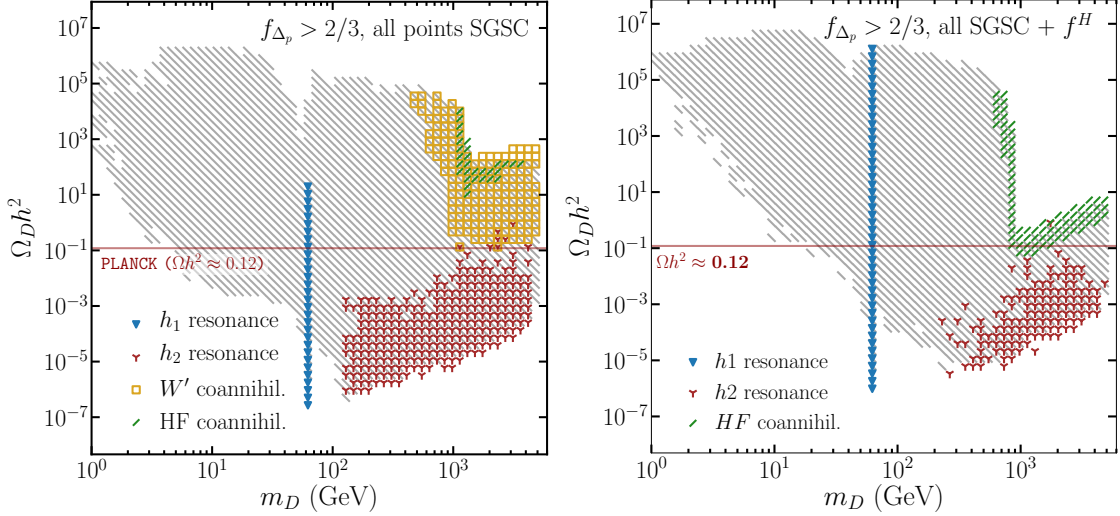


FIG. 2. The left panel describes triplet-like DM **SGSC** surviving regions projected on $(m_D, \Omega_D h^2)$ adopted from [29]. This figure neglects heavy fermions contributions. The inclusion of heavy fermions (with 5% mass splitting) is depicted on the right panel. For both cases, the gray area is ruled out by PLANCK measurement at 2σ .

this region, the DM annihilation cross section is dominated by the following processes: $DD^* \rightarrow c\bar{c}, \tau^+\tau^-$ and $b\bar{b}$, occurring mainly via the s -channel of the Higgs bosons exchange. This can be understood based on the DD^*h_i coupling in Eq. (A2). Thanks to the large value of v_Φ , the h_2 (δ_3 -like) mediated diagram is equally as important as the h_1 (SM-like) exchange while the heaviest Higgs h_3 (ϕ_2 -like) remains subdominant [29]. The observed relic abundance can be achieved in this wide range ($12 \text{ GeV} < m_D < 62 \text{ GeV}$) due to the various combinations for the DD^*h_i coupling in Eq. (A2). However, this picture is only valid when heavy fermions are neglected (the left panel of Fig. 2). Once they are included (the right panel of Fig. 2), the t -channel of heavy fermions exchange becomes relevant. There is a cancellation between the Higgs and new

heavy fermions mediated diagrams which reduces the value of DM annihilation cross section. This enhances the relic density as shown in the right panel of Fig. 2 where the gray points are shifted above the horizontal red line. The observed relic density is achieved in the mass range between 54 GeV to 62 GeV.

- (ii) When DM mass approaches half of the SM Higgs mass ($m_D \approx 62.5$ GeV), the interactions involving the s-channel of h_1 exchange become dominant. This enhances the annihilation cross section resulting in the suppression of the relic density. However, due to the wide variation of the DD^*h_1 coupling in Eq. (A2), the observed relic abundance can still be achieved. This is also true for h_2 resonance. In this case, the resonance appears in a broad range of DM mass thanks to the arbitrary values of m_{h_2} ($m_{h_2} > m_{h_1}$). Note that there is no SM Z resonance because its coupling is suppressed by $(\mathcal{O}_{32}^D)^2 \mathcal{O}_{21}^G$ as can be seen from Eq. (A1).
- (iii) Above the SM Higgs resonance, $m_{h_1}/2 < m_D < 500$ GeV, the major contributions to the DM annihilation cross section are given by W^+W^- (more than $\sim 50\%$), h_1h_1 ($\sim 25\%$), and ZZ ($\sim 20\%$) final states [29]. In all of these final states, the main contributions come from the h_1 and h_2 exchanges which lead to the S -wave cross section. On the other hand, the Z_i mediated diagrams relevant for W^+W^- final states are P - wave suppressed.
- (iv) Next, for heavy DM mass regime ($m_D > 500$ GeV), the dominant final states are given by the longitudinal parts of the SM gauge bosons, $W_L^+W_L^-$ and Z_LZ_L . However, this is only valid if one neglects heavy fermions contribution. This picture changes in the mass regime larger than 1 TeV in the presence of heavy fermions.
- (v) Finally, in the TeV region ($m_D > 1$ TeV), heavy fermions coannihilations start

to dominate. This can be seen from the right panel of Fig. 2. The main coannihilation channels in this regime are given by heavy quarks annihilations into a pair of SM quark-anti quark and gluons: $q^H \bar{q}^H \rightarrow q\bar{q}, gg$. Based on the points that we collect from our scan, these processes contribute around 87% in this regime. This is expected since these are the QCD interactions controlled by the strong coupling α_S . The main diagrams associated with these interactions are given by the s-channel of gluon exchange for $q\bar{q}$ final states and the s-channel of gluon exchange, t- and u-channel of q^H exchange for gg final states.

In Ref. [29], the relevant diagrams for the spin independent DM-nucleon interactions are given by the t-channel of h_i and Z_i exchange as displayed in the upper part of Fig. 1. The leading contribution comes from h_1 mediator while h_2, Z , and Z' mediators give non-negligible effects. This is summarized in the left panel of Fig. 3, adopted from [29]. The XENON1T limit is described by the solid red curve which assumes $f_n/f_p = 1$. The orange points in this figure are allowed by the relic density and direct detection constraints. As one can see, for DM mass larger than 300 GeV, both constraints can be evaded. As a result of ISV originating from Z and Z' exchange, there are some orange points which are located slightly above the XENON1T exclusion limit. As a comparison, the corresponding XENON1T limit for $f_n/f_p = -0.5$ is also shown.

On the other hand, when heavy fermions contribution is considered, one needs to include all diagrams in Fig. 1. There is a destructive interference between heavy quarks and the Higgs mediated diagrams. This cancellation can be extracted from the sum of these diagrams as

$$\mathcal{A}_{(q^H+h_i)} \propto \left[\frac{m_{q^H} (\mathcal{O}_{12}^D)^2}{v_\Phi^2} + \frac{m_q \mathcal{O}_{1i} \lambda_{DD^*h_i}}{v m_{h_i}^2} \right], \quad (27)$$

where m_q stands for the mass of the SM quarks. The index i runs from 1 to 2 denoting the contributions from the Higgs h_1 and h_2 while the coupling $\lambda_{DD^*h_i}$ is

given by Eq. (A2). The first term on the right hand side of Eq. (27) is always positive while the second two terms, for both h_1 and h_2 , are mostly negative.

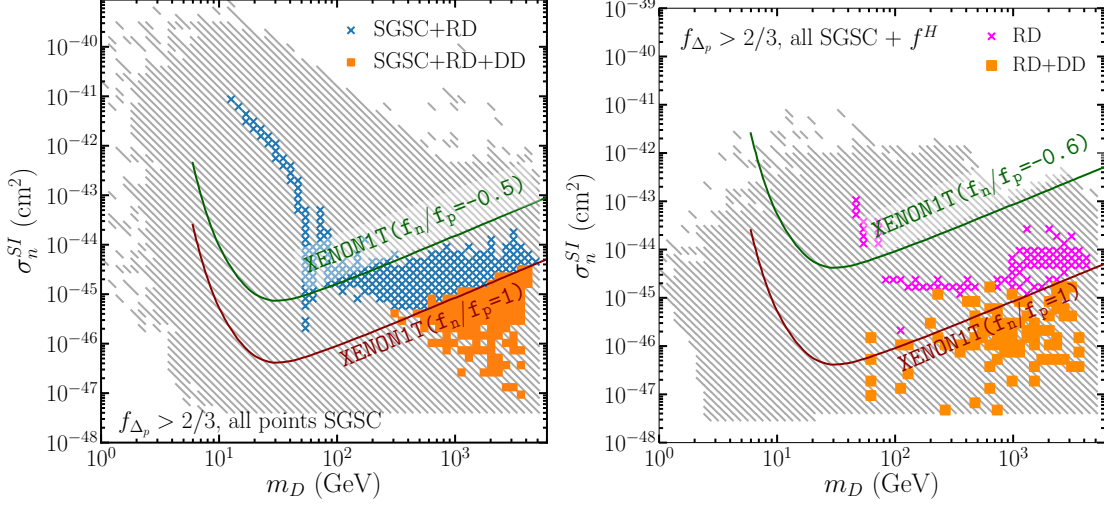


FIG. 3. In the right panel, adopted from [29] (without heavy fermions), the red solid curve is the official XENON1T exclusion limit without ISV, while the green solid curve describes the same limit with ISV value $f_n/f_p = -0.5$. Heavy fermions contribution is shown in the right panel. Here, the green solid line is XENON1T limit with $f_n/f_p = -0.6$. For both figures, the orange filled squares pass both **RD** and **DD** constraints.

This effect can be seen from the right panel of Fig. 3 where most of the gray points are located below 10^{-42}cm^2 . Interestingly, this cancellation shifts the allowed DM mass (orange squares area) towards the lighter region, reaching up to 54 GeV. There are some gaps between 60 GeV and 100 GeV as well as 140 GeV and 200 GeV where none of the points survive both relic density and direct detection constraints. This is because the cancellation given by Eq. (27) does not work effectively in this regime. In addition, the existence of the orange points significantly above the XENON1T limit shows the importance of the Z and Z' exchange when this cancellation happens

efficiently.

We see that for triplet-like DM, the inclusion of heavy fermions put a stronger constraint on the observed relic abundance, especially in the TeV regime. In contrast, they reduce the DM-nucleon spin independent cross section alleviating the current limit from XENON1T experiment.

SU(2)_H Goldstone boson-like DM

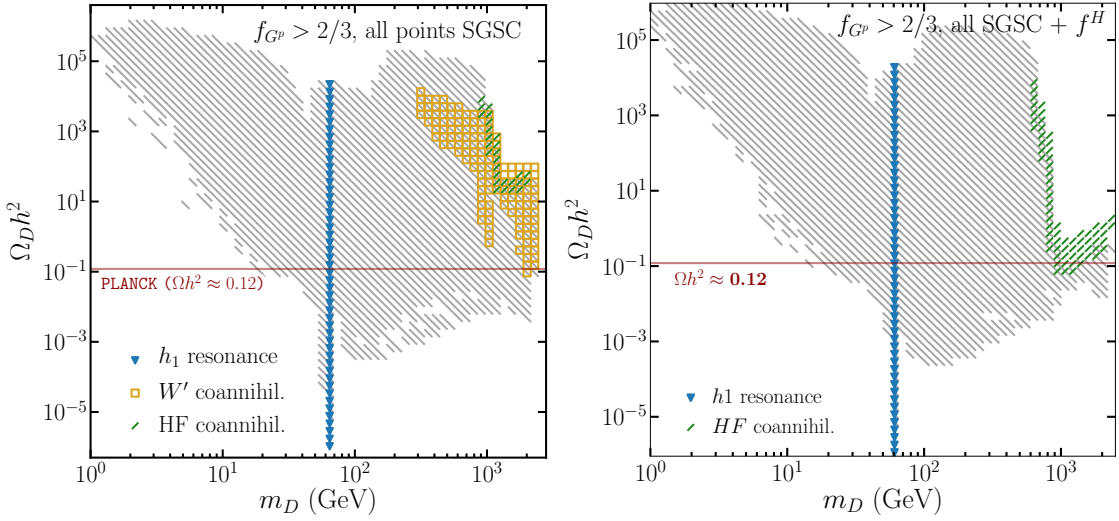


FIG. 4. The left panel shows Goldstone-like DM **SGSC** allowed regions projected on $(m_D, \Omega_D h^2)$. This figure, adopted from Ref. [29], neglects heavy fermions contributions. In contrast, the figure in the right panel takes heavy fermions into account which reduce the relic density in the TeV regime.

As we mentioned before, the Goldstone-like DM is dominated by G_H^p . However, in this particular case, the allowed composition lies in a very narrow regime between $0.67 < f_{G^p} < 0.8$. As a result, this DM lives in a tiny region in the parameter space of

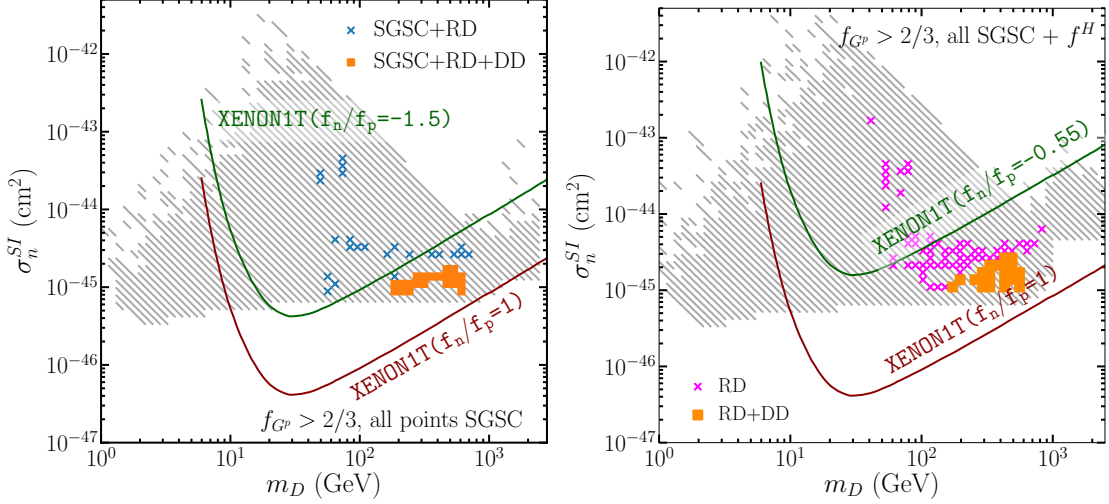


FIG. 5. The left panel is taken from [29] which omits heavy fermions. They are included in the figure on the right panel. The red solid curve, in both figures, is the XENON1T limit without ISV. The green solid line in the left (right) describes the XENON1T exclusion line with ISV value $f_n/f_p = -1.5$ ($f_n/f_p = -0.55$). The small region of orange squares shows the fine-tuned region with $f_n/f_p = -1.86$ for the left panel and $f_n/f_p = -2.00$ for the right panel. These areas are allowed by **RD** and **DD** constraints.

G2HDM model. In the left panel of Fig. 4, we show the scatter plot of the DM relic abundance with respect to its mass. The underlying physics in each mass regime (regions (i)-(iv)) is mostly similar to the triplet case [29]. Moreover, when heavy fermions are included, as shown in the right panel of Fig. 4, they strongly dominate the coannihilation channels in TeV regime as in triplet-like DM case (region (v)). Furthermore, there is no cancellation between Higgs and heavy fermions exchange thanks to the limited parameter space.

The scatter plot for DM-neutron cross section versus DM mass in the absence of heavy fermions is presented in the left panel of Fig. 5. The leading diagram is given by

the t-channel of h_1 exchange which is significant in the mass range between 3 GeV and 100 GeV. The next important diagrams come from Z' and Z exchange [29]. These ISV diagrams are relevant for DM mass larger than 100 GeV. As a result of the interference between these three dominant diagrams, the spin independent cross section varies in a wide range. However, only the orange points in the mass range $200 \text{ GeV} \leq m_D \leq 600 \text{ GeV}$ satisfy both constraints from the observed relic density and the published XENON1T limit. These points have $f_n/f_p = -1.86$ thanks to the fine-tuned parameter space. As shown in the right panel of Fig. 5, the inclusion of heavy fermions does not significantly change this result. They enhance the Z' and Z mediated diagrams shifting the ISV value of the orange region to have $f_n/f_p = -2.0$. This enhancement can also be seen in the TeV regime where the gray points are shifted upward.

V. QCD SOMMERFELD CORRECTION AND BOUND STATE FORMATION

Based on the previous section, we see that the contributions of heavy fermions are quite significant, especially in the TeV regime of the DM mass. In this case, for both triplet-like and Goldstone-like DM, heavy quarks annihilations ($q^H \bar{q}^H \rightarrow q\bar{q}, gg$) strongly reduce the relic abundance due to the QCD interactions. Since these processes occur in the early universe, at energy scale much higher than the quark-hadron phase transition era, heavy quarks experience a long range interaction via gluon exchange. This interaction can be described by Coulomb-like potential as [67]

$$V(r) = -\frac{\zeta'}{r}, \quad \zeta' = (C_{q^H} - \frac{3}{2})\alpha_s, \quad (28)$$

where ζ' describes the modified coupling between q^H and \bar{q}^H free pair which depends on the quadratic Casimir coefficient of the color representation of the heavy quark

C_{q^H} . The presence of the Coulomb-like potential modifies the perturbative calculation. This effect is known as the Sommerfeld correction [68]. For heavy quarks, the value of C_{q^H} is equal to $4/3$ since they belong to the color triplet representation of $SU(3)_C$. Furthermore, the presence of this potential may induce the bound state formation of $q^H \bar{q}^H$ pairs in the early universe [69–87]. Therefore, one needs to consider these two effects when calculating the DM abundance. In this work, we follow the method introduced in [87] for our QCD Sommerfeld correction and QCD bound state effect calculation.

A. QCD Sommerfeld Correction

The thermally averaged S - and P -wave annihilation cross sections of $q^H \bar{q}^H$ into pair of SM quark and gluons can be expanded as

$$\langle \sigma v_{rel} \rangle = a + b (T/m_{q^H}) + \mathcal{O}((T/m_{q^H})^2), \quad (29)$$

where a and b denote the S - and P -wave term, respectively. For $q\bar{q}$ final state, the corresponding expression is given by [87–89]

$$\langle \sigma v_{rel} \rangle_{q\bar{q}} = \frac{\pi \alpha_s^2}{m_{q^H}^2} \left[\frac{4}{3} - \frac{14}{3} (T/m_{q^H}) \right], \quad (30)$$

while for gluon pair final state, the associated cross section is

$$\langle \sigma v_{rel} \rangle_{gg} = \frac{\pi \alpha_s^2}{m_{q^H}^2} \left[\frac{7}{27} + \frac{1}{6} (T/m_{q^H}) \right]. \quad (31)$$

In general, the presence of the Coulomb potential of the form $V(r) = -\alpha/r$ will affect both S - and P -wave terms. For the S -wave term, it becomes $a S(\alpha/v_{rel})$ where

$$S(\alpha/v_{rel}) = \frac{2\pi \alpha/v_{rel}}{1 - e^{-2\pi\alpha/v_{rel}}}, \quad (32)$$

where v_{rel} stands for the relative velocity between q^H and \bar{q}^H . The Sommerfeld correction enhances the annihilation cross section if the potential is attractive ($\alpha > 0$) while the suppression occurs when the potential is repulsive ($\alpha < 0$). Taking this correction into account in the early universe, we need to evaluate the thermally-averaged Sommerfeld S -wave cross section as

$$a \langle S(\alpha/v_{rel}) \rangle = a \int_0^\infty S(\alpha/v_{rel}) f(v_{rel}) dv_{rel}, \quad (33)$$

where the velocity distribution $f(v_{rel})$ is given by the Maxwell-Boltzmann distribution

$$f(v_{rel}) = \left(\frac{\mu}{2\pi T}\right)^{3/2} 4\pi v_{rel}^2 e^{-\frac{\mu v_{rel}^2}{2T}}, \quad (34)$$

where $\mu = m_{q^H}/2$ and T are the reduced mass of the $q^H \bar{q}^H$ system and the temperature, respectively. In this work, we only consider the Sommerfeld correction in the S -wave term.

Following two body color decomposition for the S -wave cross section, the thermally averaged Sommerfeld corrections are [85]

$$\begin{aligned} \langle \sigma v_{rel}(q^H \bar{q}^H \rightarrow gg) \rangle_{s,Somm} &= \langle \sigma v_{rel} \rangle_{s,gg} \left(\frac{2}{7} \left\langle S\left(\frac{4\alpha_s/3}{v_{rel}}\right) \right\rangle + \frac{5}{7} \left\langle S\left(\frac{-\alpha_s/6}{v_{rel}}\right) \right\rangle \right) \\ \langle \sigma v_{rel}(q^H \bar{q}^H \rightarrow q\bar{q}) \rangle_{s,Somm} &= \langle \sigma v_{rel} \rangle_{s,q\bar{q}} \left\langle S\left(\frac{-\alpha_s/6}{v_{rel}}\right) \right\rangle, \end{aligned} \quad (35)$$

where $\langle \sigma v_{rel} \rangle_{s,q\bar{q}}$ and $\langle \sigma v_{rel} \rangle_{s,gg}$ denote the S -wave part of Eq. (30) and Eq. (31), respectively.

B. QCD Bound State Formation

When q^H and \bar{q}^H form a bound state η , the Coulomb-like potential due to gluon exchange becomes

$$V(r) = -\frac{\zeta}{r}, \quad (36)$$

$$\zeta = \frac{1}{2}(C_{q^H} + C_{\bar{q}^H} - C_\eta)\alpha_s, \quad (37)$$

where C_η is the quadratic Casimir operator of the $q^H \bar{q}^H$ bound state in a particular color state. Here, we focus on the color singlet bound state where $C_\eta = C_1 = 0$. Furthermore, we only consider bound states with total angular momentum $L = 0$ and spin $S = 0$. The corresponding binding energy of the bound state E_B and its Bohr radius a are

$$E_B = \frac{\zeta^2 \mu}{2}, \quad (38)$$

$$a = (\zeta \mu)^{-1}, \quad (39)$$

where $\mu = m_{q^H}/2$ is the reduced mass of the q^H and \bar{q}^H system.

To calculate the bound state formation cross section, one needs to know the integrated dissociation cross section first. A q^H and \bar{q}^H bound state can be destroyed by absorbing a gluon. The dissociation cross section averaged over the incoming gluon color is

$$\sigma_{dis} = \frac{1}{8} \times \frac{4}{3} \times \frac{2^9 \pi^2}{3} \alpha_s a^2 \left(\frac{E_B}{\omega} \right)^4 \frac{1 + \nu^2}{1 + (\kappa \nu)^2} \frac{e^{-4\nu \operatorname{arccot}(\kappa \nu) - 2\pi \nu}}{1 - e^{-2\pi \nu}} \kappa^{-1}. \quad (40)$$

In this expression we define ν , κ , and ω as

$$\nu \equiv \frac{|\zeta'|}{v_{rel}} \quad \kappa \equiv \frac{\zeta}{|\zeta'|} \quad \omega \approx E_B + \frac{1}{2} \mu v_{rel}^2. \quad (41)$$

Eq. (40) describes the dissociation cross section of a bound state after absorbing a gluon with energy ω . The first factor in this equation is the averaged over incoming

gluon color while the second number denotes the color factor of the bound state wave function. The bound state formation cross section can be obtained by using the Milne relation as

$$\sigma_{bsf} = \frac{g_\eta g_g \omega^2}{g_{q^H} g_{\bar{q}^H} (\mu v_{rel})^2} \sigma_{dis}, \quad (42)$$

where $g_g = 16$, $g_{q^H} = g_{\bar{q}^H} = 6$, and $g_\eta = 1$ are the degree of freedom of gluon, q^H , \bar{q}^H , and color singlet bound state, respectively.

In addition, a q^H and \bar{q}^H bound state can experience annihilation decay and individual decay of each q^H (\bar{q}^H). In the former case, the q^H and \bar{q}^H annihilate into the SM particles while in the latter case, each q^H (\bar{q}^H) decays into DM and SM particle. Thanks to the 5% mass splitting between the DM and heavy quarks, the latter process is suppressed. Additionally, this decay channel is further suppressed by $(\mathcal{O}_{12}^D)^2$. Therefore, in our case, we only need to consider the annihilation decay channel. The main decay mode is given by two gluon final state [90]

$$\Gamma_\eta^{q^H} = \frac{2}{3} \mu \alpha_s^2 \zeta^3. \quad (43)$$

Note that in Eq. (43), the explicit strong coupling α_s is evaluated at the scale of $2m_{q^H}$ while the inverse Bohr radius a^{-1} is used when evaluating the α_s dependence in ζ .

Considering the DM relic, we have to take the thermal average of the bound state effect. To get rid of the temperature dependence when evaluating the thermal average, we define $z \equiv E_B/T$ and $u \equiv \frac{1}{2} \mu v_{rel}^2/T$ such that we can express σ_{dis} and σ_{bsf} in terms of z and u . The bound state dissociation rate after taking the thermal averaging into account is

$$\langle \Gamma_\eta^{q^H} \rangle_{dis} = g_g \frac{4\pi}{(2\pi)^3} \int_0^\infty \sigma_{dis} \frac{E_B^3 (1 + \frac{u}{z})^2}{z(e^{z+u} - 1)} du. \quad (44)$$

The thermally-averaged bound state formation cross section times velocity is given by

$$\langle \sigma v \rangle_{bsf} = \int_0^\infty \sigma_{bsf} \zeta \left(\frac{u}{z} \right)^{1/2} \frac{2}{\sqrt{\pi}} u^{1/2} e^{-u} \left(1 + \frac{1}{e^{z+u} - 1} \right) du. \quad (45)$$

Finally, the thermally-averaged bound state annihilation decay rate is written as

$$\langle \Gamma_\eta^{qH} \rangle = \Gamma_\eta^{qH} \frac{K_1(m_\eta/T)}{K_2(m_\eta/T)}, \quad (46)$$

where $m_\eta = 2m_{q^H} - E_B$ and $K_{1,2}(m_\eta/T)$ are the bound state mass and the modified Bessel functions of the second kind, respectively.

Taking both Sommerfeld correction as well as bound state effect into account, we write the thermally-averaged effective annihilation cross section $\langle \sigma_{eff} v \rangle$ as

$$\langle \sigma_{eff} v \rangle = \frac{1}{2} \langle \sigma v \rangle_{q^H \bar{q}^H \rightarrow q \bar{q}, gg} \frac{g_{q^H}^2 (1 + \Delta)^3 e^{-2\Delta x}}{g_{eff}^2}. \quad (47)$$

In this expression, we have defined the following parameters

$$x \equiv \frac{m_D}{T}, \quad (48)$$

$$\Delta \equiv \frac{m_{q^H} - m_D}{m_D}, \quad (49)$$

$$g_{eff} \equiv g_D + g_{q^H} (1 + \Delta)^{3/2} e^{-\Delta x}, \quad (50)$$

where $g_D = 6$ is the DM degree of freedom. The explicit expression of $\langle \sigma v \rangle_{q^H \bar{q}^H \rightarrow q \bar{q}, gg}$ is given by

$$\begin{aligned} \langle \sigma v \rangle_{q^H \bar{q}^H \rightarrow q \bar{q}, gg} &= \langle \sigma v_{rel}(q^H \bar{q}^H \rightarrow q \bar{q}) \rangle_{s, Somm} + \langle \sigma v_{rel}(q^H \bar{q}^H \rightarrow gg) \rangle_{s, Somm} \\ &+ \langle \sigma v_{rel}(q^H \bar{q}^H \rightarrow q \bar{q}) \rangle_p + \langle \sigma v_{rel}(q^H \bar{q}^H \rightarrow gg) \rangle_p \\ &+ \frac{1}{4} \langle \sigma v_{rel} \rangle_{bsf} \frac{\langle \Gamma_\eta^{qH} \rangle}{\langle \Gamma_\eta^{qH} \rangle + \frac{1}{4} \langle \Gamma_\eta^{qH} \rangle_{dis}}, \end{aligned} \quad (51)$$

where $\langle \sigma v_{rel}(q^H \bar{q}^H \rightarrow q\bar{q}) \rangle_p$ and $\langle \sigma v_{rel}(q^H \bar{q}^H \rightarrow gg) \rangle_p$ stand for the P - wave part of the Eq. (30) and (31). The factor of 1/4 in front of $\langle \sigma v_{rel} \rangle_{bsf}$ and $\langle \Gamma_\eta^{q^H} \rangle_{dis}$ is needed since we only consider the $S = 0$ bound state. The DM relic abundance can be calculated by [91]

$$\Omega_D h^2 \cong \frac{x_f \times 1.07 \times 10^9 \text{ GeV}^{-1}}{g_*^{1/2} m_{\text{Pl}} \langle \sigma_{eff} v \rangle}, \quad (52)$$

where x_f , g_* , and m_{Pl} are the value of x at the freeze-out temperature, the number of massless degree of freedom associated with the energy density, and the Planck mass, respectively. In this work, we take all the 6 heavy quarks (u^H , d^H , s^H , c^H , b^H , and t^H) into account when calculating the Sommerfeld correction as well as bound state effect. Furthermore, we only consider one point from our scan to see how these two effects change our results. This is reasonable because $q^H \bar{q}^H \rightarrow q\bar{q}, gg$ annihilation cross sections populate 87% of our scan points in the TeV regime.

The effects of QCD Sommerfeld correction and QCD bound state on DM relic density are shown in Fig. 6. The gray band in this figure represents the observed DM relic from PLANCK collaboration within 2σ significance. The red solid curve comes from the perturbative calculation given in Eq. (30) and Eq. (31). The Sommerfeld correction, as described by the green solid curve, reduces the perturbative cross section due to the cancellation between the Sommerfeld enhancement in $q^H \bar{q}^H \rightarrow gg$ and the Sommerfeld suppression for $q^H \bar{q}^H \rightarrow q\bar{q}$ channels [67]. As a result, it increases the DM relic density, shifting the observed relic towards the smaller DM mass.

The vertical dashed lines in Fig. 6 denote the lower bound of DM mass that satisfies the observed relic abundance. The black dashed line is located at 2680 GeV. This corresponds to the perturbative calculation. At 2600 GeV, the orange dashed line comes from the Sommerfeld correction. This 3% shift demonstrates that the Sommerfeld correction does not significantly affect the DM relic abundance. The bound state effect along with the Sommerfeld correction is shown by the blue solid

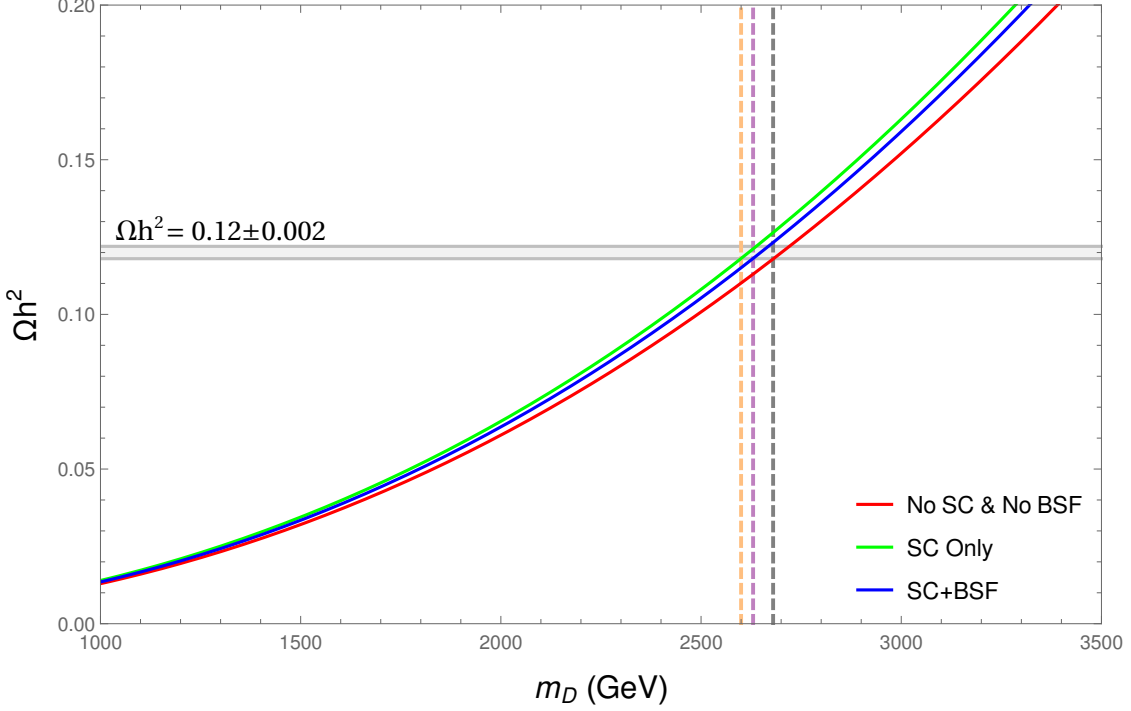


FIG. 6. DM relic density plotted against its mass for three different cases: perturbative calculation (red solid line) without Sommerfeld correction (SC) and bound state formation (BSF), perturbative calculation with SC in S -wave (green solid line), and by considering both SC and BSF (blue solid line). The gray band is the observed PLANCK data within 2σ .

curve. The lower bound of the DM mass is shifted from 2600 GeV to 2630 GeV as given by the purple dashed line. This shows that the bound state effect, in contrast to the Sommerfeld effect, slightly reduces the DM relic density.

When the electric charge of each q^H and \bar{q}^H , Q_{q^H} , is considered, the Coulomb-like potential between them becomes more attractive. This electromagnetic (EM) correction modifies the coupling of the corresponding Coulomb-like potentials as $\zeta \rightarrow \zeta + \alpha_{\text{EM}} Q_{q^H}^2$ and $\zeta' \rightarrow \zeta' + \alpha_{\text{EM}} Q_{q^H}^2$, where α_{EM} is the EM fine structure

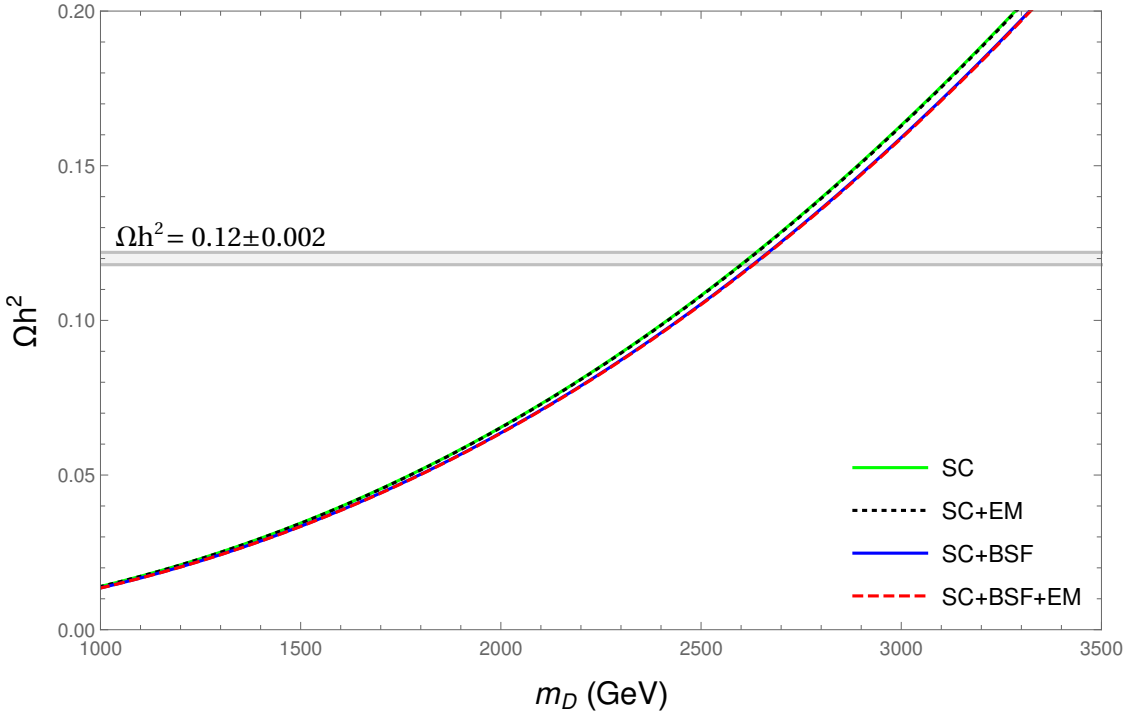


FIG. 7. The EM correction for Sommerfeld correction (SC) is given by the black dotted line. The red dashed line represents the EM correction for both SC and bound state effect (BSF). The gray band is the observed relic density from PLANCK collaboration within 2σ

constant. All quantities depending on these couplings are changed as well. The EM correction for both Sommerfeld and the bound state effects are shown in Fig. 7. As in Fig. 6, the green (blue) solid curve describes the Sommerfeld (Sommerfeld and the bound state) effect. The black dotted curve is the EM correction of the Sommerfeld effect. This weakens the value of the relic density by 0.15% at 2600 GeV. Furthermore, another similar reduction is also observed when one considers the EM correction of the bound state effect along with the Sommerfeld correction. This is shown by the red dashed curve in Fig. 7. In this case, the reduction of the

relic density is about 0.17% at 2630 GeV. These results demonstrate that the EM correction is negligibly small and can be omitted in the calculation of the DM relic abundance.

We see that non-perturbative effects such as the QCD Sommerfeld correction as well as the QCD bound state effect do not significantly change the DM relic abundance. Thus, one can safely ignore these effects and carry out the perturbative calculation given by Eq. (30) and Eq. (31).

VI. CONSTRAINING PARAMETER SPACE IN G2HDM

We see from the preceding sections that the Goldstone-like DM lives in the limited parameter space region. Moreover, the particular value of $f_n/f_p \approx -2.00$ is needed to avoid the XENON1T limit. Thus, in this subsection, we focus our discussion on the triplet-like DM when evaluating the surviving parameter space in G2HDM.

We collect the allowed parameter regions from the **SGSC+RD+DD** constraints in table IV and V. In this work, the allowed parameter regions are collected in the right column of these tables. The left column lists the surviving parameter space from [29]. As a general remark, we see that the inclusion of heavy fermions put the allowed parameter space into the smaller region.

As discussed in [29], the **RD+DD** constraints put a strong limits on $\lambda_{\Phi\Delta}$, $\lambda_{H\Delta}$, and $\lambda_{\Phi\Delta}$. This can be seen from their explicit appearance in DD^*h_j couplings in Eq. (A2). Due to its correlation with $\lambda_{\Phi\Delta}$, these constraints restrict λ_{Φ} as well. As a consequence of the loose requirement that we impose on triplet-like DM, $f_{\Delta_p} > 2/3$, the G_H^p component becomes non-negligible. In fact, there are points with $G_H^p = 1/3$ in our scan. Consequently, this constraints $\lambda_{H\Phi}$ and $\lambda'_{H\Phi}$ which are relevant for the $f_{G_H^p}$ component as one can see from Eq. (A4). Furthermore, there are indirect constraints on other parameters due to the mixing angles which appear in Eq. (A2)

Allowed Parameter Ranges without f^H	Allowed Parameter Ranges with f^H
$6.35 \times 10^{-3} < \lambda_\Phi < 4.09$	$4.24 \times 10^{-3} < \lambda_\Phi < 3.98$
$-3.39 < \lambda_{H\Delta} < 4.07$	$-3.16 < \lambda_{H\Delta} < 4.16$
$-0.07 < \lambda_{\Phi\Delta} < 6.62$	$-0.30 < \lambda_{\Phi\Delta} < 6.10$
$-5.67 < \lambda_{H\Phi} < 3.41$	$-5.33 < \lambda_{H\Phi} < 2.54$
$-0.01 < \lambda'_{H\Phi} < 15.90$	$0.01 < \lambda'_{H\Phi} < 14.36$
$1.29 \times 10^{-1} < \lambda_H < 2.80$	$1.30 \times 10^{-1} < \lambda_H < 2.69$
$-22.74 < \lambda'_H < 9.57$	$-21.75 < \lambda'_H < 7.61$
$1.01 \times 10^{-4} < \lambda_\Delta < 4.99$	$1.20 \times 10^{-4} < \lambda_\Delta < 4.84$
$7.16 \times 10^{-3} < g_H < 0.10$	$3.37 \times 10^{-3} < g_H < 0.10$
$1.01 \times 10^{-8} < g_X < 3.55 \times 10^{-2}$	$1.01 \times 10^{-8} < g_X < 3.01 \times 10^{-2}$

TABLE IV. The surviving parameter space after DM constraints.

and Eq. (A4).

From previous sections, especially the relic density of triplet-like DM, we see the importance of the DD^*h_j couplings. In [29], these couplings play important role in the relic density calculation for all DM mass. However, these couplings are relevant only in the GeV regime (region (i) to (iv)) when heavy fermions are included. This significantly cuts the allowed parameter space in G2HDM. The same reduction also holds for g_H and g_X . These two couplings correspond to the Z_i mediated diagrams, especially for W^+W^- as well as $W_L^+W_L^-$ final states in region (iii) and (iv) (although these contributions are P -wave suppressed). Furthermore, g_H and v_Φ receive additional constraints from the lower allowed DM mass as in Eq. (25).

Finally, the constraints from DM physics are not sensitive to limit v_Δ , $M_{\Phi\Delta}$, and $M_{H\Delta}$. In this paper, we extend the scan range for $M_{H\Delta}$ to include the negative values of the parameter space. The motivation is to collect more points in our scan. This

Allowed Parameter Ranges without f^H (in GeV)	Allowed Parameter Ranges with f^H (in GeV)
$2.75 < M_{H\Delta} < 4.99 \times 10^3$	$-2.44 \times 10^3 < M_{H\Delta} < 4.51 \times 10^3$
$0.01 < M_{\Phi\Delta} < 49.9$	$0.00 < M_{\Phi\Delta} < 49.8$
$5.00 \times 10^2 < v_\Delta < 2.00 \times 10^4$	$5.07 \times 10^2 < v_\Delta < 1.99 \times 10^4$
$4.15 \times 10^4 < v_\Phi < 1.00 \times 10^5$	$3.99 \times 10^4 < v_\Phi < 9.99 \times 10^4$

TABLE V. The surviving dimensionful parameter space after DM constraints.

explains the broader allowed parameter range for $M_{H\Delta}$ as one can see from table V.

VII. SUMMARY AND CONCLUSION

The motivation of this paper is to study the effects of heavy fermions on the complex scalar DM phenomenology which is omitted in the previous work. Taking the constraints from the observed relic abundance provided by PLANCK collaboration as well as the null result from XENON1T experiment into account, we compare our calculations against these experimental data. By imposing 5% mass splitting between the DM and heavy fermions as well as lowering their mass to 1 TeV, we demonstrate that the heavy fermions significantly affect the complex scalar DM phenomenology. The DM relic abundance is reduced drastically in the TeV regime of the DM mass. This happens mainly because of the QCD interactions, $q^H \bar{q}^H \rightarrow q\bar{q}, gg$.

We further include the QCD Sommerfeld correction as well as the QCD bound state effect in our relic density calculation. We learn that these non-perturbative effects do not change the perturbative calculation in a significant way. On the other hand, heavy fermions weaken the direct search limit given by the XENON1T experiment. This is due to their destructive contribution in the relevant Feynman diagrams. These results put additional constraints on the parameter space of the

G2HDM model. This makes the allowed region in the parameter space becomes narrower. We conclude that the inclusion of heavy fermions on the complex scalar DM phenomenology is crucial and can not be neglected.

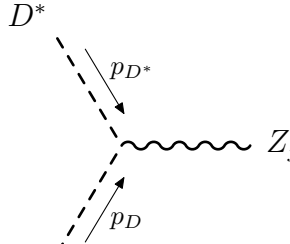
ACKNOWLEDGMENTS

We would like to thank Prof. Tzu-Chiang Yuan who encourages the author to write this paper. CSN would like to thank Prof. Hsiang-Nan Li for useful discussions regarding the evaluation of the strong coupling at different scale in QCD bound state effect. BD would like to acknowledge support from Thailand Science Research and Innovation and Suranaree University of Technology through SUT-Ph.D. Scholarship Program for ASEAN.

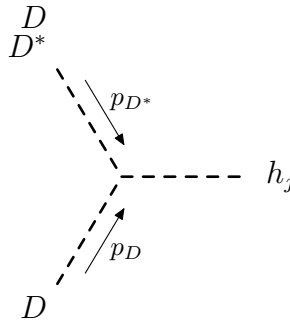
Appendix A: Feynman Rules

Here we collect the most important couplings to the DM analysis in various interactions as discussed in the text. The gauge couplings g_H and g_X are related to $SU(2)_H$ and $U(1)_X$ gauge group, respectively. For the scalar-scalar-gauge derivative vertices, we use the convention that all momenta are incoming.

Dominant Couplings for Triplet-like DM

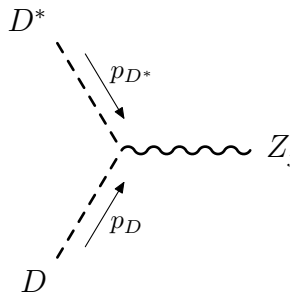


$$\approx ig_H (\mathcal{O}_{32}^D)^2 \mathcal{O}_{2j}^G (p_{D^*} - p_D)_\mu \quad (\text{A1})$$



$$\approx i [-\lambda_{H\Delta} v \mathcal{O}_{1j} - \lambda_{\Phi\Delta} v_\Phi \mathcal{O}_{2j} + 2\lambda_{\Delta} v_\Delta \mathcal{O}_{3j}] (\mathcal{O}_{32}^D)^2 \quad (\text{A2})$$

Dominant Couplings for Goldstone boson-like DM



$$\approx i \left[\frac{g_H}{2} \mathcal{O}_{2j}^G + g_X \mathcal{O}_{3j}^G \right] (\mathcal{O}_{12}^D)^2 (p_{D^*} - p_D)_\mu \quad (\text{A3})$$

$$\begin{array}{c}
 D^* \\
 \swarrow p_{D^*} \\
 \text{---} h_j \approx i [-(\lambda_{H\Phi} + \lambda'_{H\Phi}) \mathcal{O}_{1j} v - 2\lambda_\Phi \mathcal{O}_{2j} v_\Phi + \lambda_{\Phi\Delta} \mathcal{O}_{3j} v_\Delta] (\mathcal{O}_{12}^D)^2 \\
 \nwarrow p_D \\
 D
 \end{array}
 \tag{A4}$$

- [1] G. C. Branco, P. M. Ferreira, L. Lavoura, M. N. Rebelo, M. Sher and J. P. Silva, Phys. Rept. **516**, 1 (2012) doi:10.1016/j.physrep.2012.02.002 [arXiv:1106.0034 [hep-ph]].
- [2] H. E. Logan, arXiv:1406.1786 [hep-ph].
- [3] N. G. Deshpande and E. Ma, Phys. Rev. D **18**, 2574 (1978). doi:10.1103/PhysRevD.18.2574
- [4] L. Lopez Honorez, E. Nezri, J. F. Oliver and M. H. G. Tytgat, JCAP **0702**, 028 (2007) doi:10.1088/1475-7516/2007/02/028 [hep-ph/0612275].
- [5] C. Arina, F. S. Ling and M. H. G. Tytgat, JCAP **0910**, 018 (2009) doi:10.1088/1475-7516/2009/10/018 [arXiv:0907.0430 [hep-ph]].
- [6] E. Nezri, M. H. G. Tytgat and G. Vertongen, JCAP **0904**, 014 (2009) doi:10.1088/1475-7516/2009/04/014 [arXiv:0901.2556 [hep-ph]].
- [7] X. Miao, S. Su and B. Thomas, Phys. Rev. D **82**, 035009 (2010) doi:10.1103/PhysRevD.82.035009 [arXiv:1005.0090 [hep-ph]].
- [8] M. Gustafsson, S. Rydbeck, L. Lopez-Honorez and E. Lundstrom, Phys. Rev. D **86**, 075019 (2012) doi:10.1103/PhysRevD.86.075019 [arXiv:1206.6316 [hep-ph]].
- [9] A. Arhrib, R. Benbrik and N. Gaur, Phys. Rev. D **85**, 095021 (2012) doi:10.1103/PhysRevD.85.095021 [arXiv:1201.2644 [hep-ph]].
- [10] A. Arhrib, R. Benbrik and T. C. Yuan, Eur. Phys. J. C **74**, 2892 (2014) doi:10.1140/epjc/s10052-014-2892-5 [arXiv:1401.6698 [hep-ph]].

- [11] B. Swiezewska and M. Krawczyk, *Phys. Rev. D* **88**, no. 3, 035019 (2013) doi:10.1103/PhysRevD.88.035019 [arXiv:1212.4100 [hep-ph]].
- [12] A. Arhrib, Y. L. S. Tsai, Q. Yuan and T. C. Yuan, *JCAP* **1406**, 030 (2014) doi:10.1088/1475-7516/2014/06/030 [arXiv:1310.0358 [hep-ph]].
- [13] A. Goudelis, B. Herrmann and O. Stål, *JHEP* **1309**, 106 (2013) doi:10.1007/JHEP09(2013)106 [arXiv:1303.3010 [hep-ph]].
- [14] M. Krawczyk, D. Sokolowska, P. Swaczyna and B. Swiezewska, *JHEP* **1309**, 055 (2013) doi:10.1007/JHEP09(2013)055 [arXiv:1305.6266 [hep-ph]].
- [15] M. Krawczyk, D. Sokolowska, P. Swaczyna and B. Swiezewska, *Acta Phys. Polon. B* **44**, no. 11, 2163 (2013) doi:10.5506/APhysPolB.44.2163 [arXiv:1309.7880 [hep-ph]].
- [16] A. Ilnicka, M. Krawczyk and T. Robens, *Phys. Rev. D* **93**, no. 5, 055026 (2016) doi:10.1103/PhysRevD.93.055026 [arXiv:1508.01671 [hep-ph]].
- [17] M. A. Diaz, B. Koch and S. Urrutia-Quiroga, *Adv. High Energy Phys.* **2016**, 8278375 (2016) doi:10.1155/2016/8278375 [arXiv:1511.04429 [hep-ph]].
- [18] K. P. Modak and D. Majumdar, *Astrophys. J. Suppl.* **219**, no. 2, 37 (2015) doi:10.1088/0067-0049/219/2/37 [arXiv:1502.05682 [hep-ph]].
- [19] T. W. Kephart and T. C. Yuan, *Nucl. Phys. B* **906**, 549 (2016) doi:10.1016/j.nuclphysb.2016.03.023 [arXiv:1508.00673 [hep-ph]].
- [20] F. S. Queiroz and C. E. Yaguna, *JCAP* **1602**, no. 02, 038 (2016) doi:10.1088/1475-7516/2016/02/038 [arXiv:1511.05967 [hep-ph]].
- [21] C. Garcia-Cely, M. Gustafsson and A. Ibarra, *JCAP* **1602**, no. 02, 043 (2016) doi:10.1088/1475-7516/2016/02/043 [arXiv:1512.02801 [hep-ph]].
- [22] M. Hashemi and S. Najjari, *Eur. Phys. J. C* **77**, no. 9, 592 (2017) doi:10.1140/epjc/s10052-017-5159-0 [arXiv:1611.07827 [hep-ph]].
- [23] P. Poulose, S. Sahoo and K. Sridhar, *Phys. Lett. B* **765**, 300 (2017) doi:10.1016/j.physletb.2016.12.022 [arXiv:1604.03045 [hep-ph]].

- [24] A. Alves, D. A. Camargo, A. G. Dias, R. Longas, C. C. Nishi and F. S. Queiroz, *JHEP* **1610**, 015 (2016) doi:10.1007/JHEP10(2016)015 [arXiv:1606.07086 [hep-ph]].
- [25] A. Datta, N. Ganguly, N. Khan and S. Rakshit, *Phys. Rev. D* **95**, no. 1, 015017 (2017) doi:10.1103/PhysRevD.95.015017 [arXiv:1610.00648 [hep-ph]].
- [26] A. Belyaev, G. Cacciapaglia, I. P. Ivanov, F. Rojas-Abatte and M. Thomas, *Phys. Rev. D* **97**, no. 3, 035011 (2018) doi:10.1103/PhysRevD.97.035011 [arXiv:1612.00511 [hep-ph]].
- [27] A. Belyaev, T. R. Fernandez Perez Tomei, P. G. Mercadante, C. S. Moon, S. Moretti, S. F. Novaes, L. Panizzi, F. Rojas and M. Thomas, *Phys. Rev. D* **99**, no. 1, 015011 (2019) doi:10.1103/PhysRevD.99.015011 [arXiv:1809.00933 [hep-ph]].
- [28] W. C. Huang, Y. L. S. Tsai and T. C. Yuan, *JHEP* **1604**, 019 (2016) doi:10.1007/JHEP04(2016)019 [arXiv:1512.00229 [hep-ph]].
- [29] C. R. Chen, Y. X. Lin, C. S. Nugroho, R. Ramos, Y. L. S. Tsai and T. C. Yuan, *Phys. Rev. D* **101**, no.3, 035037 (2020) doi:10.1103/PhysRevD.101.035037 [arXiv:1910.13138 [hep-ph]].
- [30] H. Davoudiasl, R. Kitano, T. Li and H. Murayama, *Phys. Lett. B* **609**, 117 (2005) doi:10.1016/j.physletb.2005.01.026 [hep-ph/0405097].
- [31] S. W. Ham, Y. S. Jeong and S. K. Oh, *J. Phys. G* **31**, no. 8, 857 (2005) doi:10.1088/0954-3899/31/8/017 [hep-ph/0411352].
- [32] W. C. Huang, Y. L. S. Tsai and T. C. Yuan, *Nucl. Phys. B* **909**, 122 (2016) doi:10.1016/j.nuclphysb.2016.05.002 [arXiv:1512.07268 [hep-ph]].
- [33] W. C. Huang, H. Ishida, C. T. Lu, Y. L. S. Tsai and T. C. Yuan, *Eur. Phys. J. C* **78**, no. 8, 613 (2018) doi:10.1140/epjc/s10052-018-6067-7 [arXiv:1708.02355 [hep-ph]].
- [34] C. R. Chen, Y. X. Lin, V. Q. Tran and T. C. Yuan, *Phys. Rev. D* **99**, no. 7, 075027 (2019) doi:10.1103/PhysRevD.99.075027 [arXiv:1810.04837 [hep-ph]].

- [35] A. Arhrib, W. C. Huang, R. Ramos, Y. L. S. Tsai and T. C. Yuan, *Phys. Rev. D* **98**, no. 9, 095006 (2018) doi:10.1103/PhysRevD.98.095006 [arXiv:1806.05632 [hep-ph]].
- [36] C. T. Huang, R. Ramos, V. Q. Tran, Y. L. S. Tsai and T. C. Yuan, *JHEP* **1909**, 048 (2019) doi:10.1007/JHEP09(2019)048 [arXiv:1905.02396 [hep-ph]].
- [37] <http://pdg.arsip.lipi.go.id/2017/reviews/rpp2016-rev-susy-2-experiment.pdf>
- [38] R. N. Mohapatra and G. Senjanovic, *Phys. Rev. Lett.* **44**, 912 (1980). doi:10.1103/PhysRevLett.44.912
- [39] W. Y. Keung and G. Senjanovic, *Phys. Rev. Lett.* **50**, 1427 (1983). doi:10.1103/PhysRevLett.50.1427
- [40] P. Q. Hung, *Phys. Lett. B* **649**, 275 (2007) doi:10.1016/j.physletb.2007.03.067 [hep-ph/0612004].
- [41] P. Q. Hung, T. Le, V. Q. Tran and T. C. Yuan, *Nucl. Phys. B* **932**, 471 (2018) doi:10.1016/j.nuclphysb.2018.05.020 [arXiv:1701.01761 [hep-ph]].
- [42] C. F. Chang, C. H. V. Chang, C. S. Nugroho and T. C. Yuan, *Nucl. Phys. B* **910**, 293-308 (2016) doi:10.1016/j.nuclphysb.2016.07.009 [arXiv:1602.00680 [hep-ph]].
- [43] P. Q. Hung, T. Le, V. Q. Tran and T. C. Yuan, *JHEP* **1512**, 169 (2015) doi:10.1007/JHEP12(2015)169 [arXiv:1508.07016 [hep-ph]].
- [44] C. F. Chang, P. Q. Hung, C. S. Nugroho, V. Tran and T. C. Yuan, *Nucl. Phys. B* **928**, 21-37 (2018) doi:10.1016/j.nuclphysb.2018.01.007 [arXiv:1702.04516 [hep-ph]].
- [45] P. Q. Hung, Y. X. Lin, C. S. Nugroho and T. C. Yuan, *Nucl. Phys. B* **927**, 166-183 (2018) doi:10.1016/j.nuclphysb.2017.12.014 [arXiv:1709.01690 [hep-ph]].
- [46] P. Ko, Y. Omura and C. Yu, *Phys. Lett. B* **717**, 202 (2012) doi:10.1016/j.physletb.2012.09.019 [arXiv:1204.4588 [hep-ph]].
- [47] M. D. Campos, D. Cogollo, M. Lindner, T. Melo, F. S. Queiroz and W. Rodejohann, *JHEP* **1708**, 092 (2017) doi:10.1007/JHEP08(2017)092 [arXiv:1705.05388 [hep-ph]].

- [48] D. A. Camargo, L. Delle Rose, S. Moretti and F. S. Queiroz, *Phys. Lett. B* **793**, 150 (2019) doi:10.1016/j.physletb.2019.04.048 [arXiv:1805.08231 [hep-ph]].
- [49] D. A. Camargo, A. G. Dias, T. B. de Melo and F. S. Queiroz, *JHEP* **1904**, 129 (2019) doi:10.1007/JHEP04(2019)129 [arXiv:1811.05488 [hep-ph]].
- [50] D. A. Camargo, M. D. Campos, T. B. de Melo and F. S. Queiroz, *Phys. Lett. B* **795**, 319 (2019) doi:10.1016/j.physletb.2019.06.020 [arXiv:1901.05476 [hep-ph]].
- [51] D. Cogollo, R. D. Matheus, T. B. de Melo and F. S. Queiroz, *Phys. Lett. B* **797**, 134813 (2019) doi:10.1016/j.physletb.2019.134813 [arXiv:1904.07883 [hep-ph]].
- [52] E. C. G. Stueckelberg, *Helv. Phys. Acta* **11**, 299 (1938).
- [53] H. Ruegg and M. Ruiz-Altaba, *Int. J. Mod. Phys. A* **19**, 3265 (2004) doi:10.1142/S0217751X04019755 [hep-th/0304245].
- [54] B. Kors and P. Nath, *JHEP* **0507**, 069 (2005) doi:10.1088/1126-6708/2005/07/069 [hep-ph/0503208].
- [55] B. Kors and P. Nath, doi:10.1142/9789812701756_0056 [hep-ph/0411406].
- [56] B. Kors and P. Nath, *JHEP* **0412**, 005 (2004) doi:10.1088/1126-6708/2004/12/005 [hep-ph/0406167].
- [57] B. Kors and P. Nath, *Phys. Lett. B* **586**, 366 (2004) doi:10.1016/j.physletb.2004.02.051 [hep-ph/0402047].
- [58] D. Feldman, Z. Liu and P. Nath, *AIP Conf. Proc.* **939**, 50 (2007) doi:10.1063/1.2803786 [arXiv:0705.2924 [hep-ph]].
- [59] D. Feldman, Z. Liu and P. Nath, *Phys. Rev. D* **75**, 115001 (2007) doi:10.1103/PhysRevD.75.115001 [hep-ph/0702123 [HEP-PH]].
- [60] D. Feldman, Z. Liu and P. Nath, *JHEP* **0611**, 007 (2006) doi:10.1088/1126-6708/2006/11/007 [hep-ph/0606294].
- [61] S. L. Glashow and S. Weinberg, *Phys. Rev. D* **15**, 1958 (1977). doi:10.1103/PhysRevD.15.1958

- [62] E. A. Paschos, Phys. Rev. D **15**, 1966 (1977). doi:10.1103/PhysRevD.15.1966
- [63] N. Aghanim *et al.* [Planck Collaboration], arXiv:1807.06209 [astro-ph.CO].
- [64] E. Aprile *et al.* [XENON Collaboration], Phys. Rev. Lett. **121**, no. 11, 111302 (2018) doi:10.1103/PhysRevLett.121.111302 [arXiv:1805.12562 [astro-ph.CO]].
- [65] G. Belanger, F. Boudjema, A. Goudelis, A. Pukhov and B. Zaldivar, Comput. Phys. Commun. **231**, 173 (2018) doi:10.1016/j.cpc.2018.04.027 [arXiv:1801.03509 [hep-ph]].
- [66] G. Belanger, F. Boudjema, A. Pukhov and A. Semenov, Comput. Phys. Commun. **180**, 747 (2009) doi:10.1016/j.cpc.2008.11.019 [arXiv:0803.2360 [hep-ph]].
- [67] S. El Hedri, A. Kaminska, M. de Vries and J. Zurita, JHEP **04**, 118 (2017) doi:10.1007/JHEP04(2017)118 [arXiv:1703.00452 [hep-ph]].
- [68] A. Sommerfeld Annals Phys. 403 (1931) 257
- [69] J. L. Feng, M. Kaplinghat, H. Tu and H. B. Yu, JCAP **07**, 004 (2009) doi:10.1088/1475-7516/2009/07/004 [arXiv:0905.3039 [hep-ph]].
- [70] B. von Harling and K. Petraki, JCAP **12**, 033 (2014) doi:10.1088/1475-7516/2014/12/033 [arXiv:1407.7874 [hep-ph]].
- [71] K. Petraki, M. Postma and M. Wiechers, JHEP **06**, 128 (2015) doi:10.1007/JHEP06(2015)128 [arXiv:1505.00109 [hep-ph]].
- [72] S. Kim and M. Laine, JHEP **07**, 143 (2016) doi:10.1007/JHEP07(2016)143 [arXiv:1602.08105 [hep-ph]].
- [73] S. Kim and M. Laine, JCAP **01**, 013 (2017) doi:10.1088/1475-7516/2017/01/013 [arXiv:1609.00474 [hep-ph]].
- [74] K. Petraki, M. Postma and J. de Vries, JHEP **04**, 077 (2017) doi:10.1007/JHEP04(2017)077 [arXiv:1611.01394 [hep-ph]].
- [75] K. Petraki, L. Pearce and A. Kusenko, JCAP **07**, 039 (2014) doi:10.1088/1475-7516/2014/07/039 [arXiv:1403.1077 [hep-ph]].

- [76] W. Detmold, M. McCullough and A. Pochinsky, *Phys. Rev. D* **90**, no.11, 115013 (2014) doi:10.1103/PhysRevD.90.115013 [arXiv:1406.2276 [hep-ph]].
- [77] H. An, M. B. Wise and Y. Zhang, *Phys. Rev. D* **93**, no.11, 115020 (2016) doi:10.1103/PhysRevD.93.115020 [arXiv:1604.01776 [hep-ph]].
- [78] C. Kouvaris, K. Langæble and N. G. Nielsen, *JCAP* **10**, 012 (2016) doi:10.1088/1475-7516/2016/10/012 [arXiv:1607.00374 [hep-ph]].
- [79] J. Ellis, F. Luo and K. A. Olive, *JHEP* **09**, 127 (2015) doi:10.1007/JHEP09(2015)127 [arXiv:1503.07142 [hep-ph]].
- [80] J. Ellis, J. L. Evans, F. Luo and K. A. Olive, *JHEP* **02**, 071 (2016) doi:10.1007/JHEP02(2016)071 [arXiv:1510.03498 [hep-ph]].
- [81] N. Nagata, H. Otono and S. Shirai, *Phys. Lett. B* **748**, 24-29 (2015) doi:10.1016/j.physletb.2015.06.044 [arXiv:1504.00504 [hep-ph]].
- [82] J. L. Feng, M. Kaplinghat and H. B. Yu, *Phys. Rev. D* **82**, 083525 (2010) doi:10.1103/PhysRevD.82.083525 [arXiv:1005.4678 [hep-ph]].
- [83] H. Iminiyaz and M. Kakizaki, *Nucl. Phys. B* **851**, 57-65 (2011) doi:10.1016/j.nuclphysb.2011.05.009 [arXiv:1008.2905 [astro-ph.CO]].
- [84] A. Hryczuk, R. Iengo and P. Ullio, *JHEP* **03**, 069 (2011) doi:10.1007/JHEP03(2011)069 [arXiv:1010.2172 [hep-ph]].
- [85] A. De Simone, G. F. Giudice and A. Strumia, *JHEP* **06**, 081 (2014) doi:10.1007/JHEP06(2014)081 [arXiv:1402.6287 [hep-ph]].
- [86] W. Y. Keung, I. Low and Y. Zhang, *Phys. Rev. D* **96**, no.1, 015008 (2017) doi:10.1103/PhysRevD.96.015008 [arXiv:1703.02977 [hep-ph]].
- [87] S. P. Liew and F. Luo, *JHEP* **02**, 091 (2017) doi:10.1007/JHEP02(2017)091 [arXiv:1611.08133 [hep-ph]].
- [88] M. Srednicki, R. Watkins and K. A. Olive, *Nucl. Phys. B* **310**, 693 (1988) doi:10.1016/0550-3213(88)90099-5

- [89] J. R. Ellis, T. Falk, K. A. Olive and M. Srednicki, *Astropart. Phys.* **13**, 181-213 (2000)
[erratum: *Astropart. Phys.* **15**, 413-414 (2001)] doi:10.1016/S0927-6505(99)00104-8
[arXiv:hep-ph/9905481 [hep-ph]].
- [90] D. Kahawala and Y. Kats, *JHEP* **09**, 099 (2011) doi:10.1007/JHEP09(2011)099
[arXiv:1103.3503 [hep-ph]].
- [91] A. Berlin, D. Hooper and S. D. McDermott, *Phys. Rev. D* **89**, no.11, 115022 (2014)
doi:10.1103/PhysRevD.89.115022 [arXiv:1404.0022 [hep-ph]].